ChemCatChem

Review
doi.org/10.1002/cctc.202400638

Chemistry Europe
European Chemical Societies Publishing

www.chemcatchem.org

A Perspective on Photocatalytic Synthesis of NH_3, Urea, and Amino Acids by Nanomaterials: Progress and Prospects

Biswajit Bhattacharyya,*[a] Radwan M. Sarhan,[b] Yan Lu,[a, b] and Andreas Taubert[a]

A sustainable world is only possible when we are ready to deliver a net zero carbon emission energy sector. In this regard, we must not only consider more renewable energy resources but also find alternate paths for making some popular molecules like NH_3 and urea for a lesser carbon footprint. This perspective article summarizes the recent progress of the photocatalytic synthesis of NH_3, urea, and some amino acids using novel nanomaterials where we have focused on various approaches to catalyst design like metal oxides, metal sulfides, metal-free catalysts, and biomimicking catalysts for ambient condition N_2 activation. Later we discussed general reaction pathways, a detailed mechanistic overview, and future material layout for a sustainable approach towards N_2 activation.

1. Introduction

The impact of climate change across the globe with its substantial increase of greenhouse gases has drastically affected our daily life.[1–4] Developing an alternate pathway for energy harvesting with a smaller carbon footprint is one of the major criteria to avoid these environmental effects.[5–8] In this regard, the scientific community is paying much more attention towards solar fuel generation.[9–13] Among the various examples, ammonia (NH_3) is one of them. It is one of the vital synthesized molecules for our living system. Its different applications have been widely spread over the various sectors of agriculture as well as chemical industries with a worth of $60 billion economy. It is also one of the important clean energy sources due to its high energy density which is almost double that of hydrogen.[14,15–17]

From 1909 onwards, the Haber–Bosch process is the only synthetic pathway to make NH_3 on an industrial scale.[18] Practically, it is a harsh method of synthesis with extreme reaction conditions where temperature and pressure have to be in the range of 350–550 °C and 150–350 atm. Besides these extreme conditions, one more problem also exists. The Haber-Bosch reaction proceeds through a dissociative pathway where the activation of both H_2 and N_2 are involved. The hydrogen gas is mainly produced by the combustion of natural gases in the presence of steam which is a grating method and produces large amounts of CO_2 as a side product. This process generates about 1 % of the world's carbon footprint.[19,20]

Although the amount of N_2 in our atmosphere is virtually unlimited, the stability and chemical inertness of N_2 triple bonds with a bond energy of 940.95 kJ/mole poses a significant challenge to fixing N_2 at ambient conditions.[21,22]

This current review article will discuss the recent advancement of photocatalytic synthesis of ammonia, urea, and some amino acids using novel semiconductors and metal nanoparticles. Various examples of materials with structural correlations, and optical properties are discussed in favor of photochemical reduction reactions to produce above-desired molecules. Finally, the challenges for large-scale production, alternate sources of N_2, and proposed future materials are put forward.

2. Biological N_2 Fixation

Biological N_2 activation occurs naturally in diazotrophic microorganisms through the enzyme nitrogenase at ambient conditions (<35 °C, atmospheric pressure).[23,24] The study of this enzyme thus has potential interest with the proper prospect for sustainable and efficient ammonia synthesis.

$$N_2 + 8H^+ + 16MgATP + 8e^- = 2NH_3 + H_2 + 16MgADP + 16Pi\ (\text{Inorganic Phosphate}) \quad (1)$$

From the basic mechanism of this particular reaction, it is very clear that every molecule of nitrogen is reduced to two molecules of ammonia with extra hydrogen ions which are also eventually reduced to hydrogen gas [reaction-1]. In the absence of nitrogen, there is only hydrogen gas generation. Three different nitrogenase enzymes have similar activities. They differ only by their metal-centered catalytic cofactors like FeMo Cofactors, FeFe Cofactors, and FeV Cofactors. Among these three, most nitrogenase enzymes contain the FeMo-Cofactors. Figure 1a presents the process of ammonia formation by the enzyme nitrogenase with its active sites.[25]

One major challenge is to understand the binding proteins and metal sulfur cluster dynamics of these cofactors. There are

[a] Dr. B. Bhattacharyya, Prof. Y. Lu, Prof. A. Taubert
Institute of Chemistry, University of Potsdam, Karl-Liebknecht-Strasse 24–25, D-14476 Potsdam, Germany
E-mail: bhattacharyya@uni-potsdam.de

[b] Dr. R. M. Sarhan, Prof. Y. Lu
Department for Electrochemical Energy Storage, Helmholtz Zentrum Berlin für Materialien und Energie, 14109 Berlin, Germany

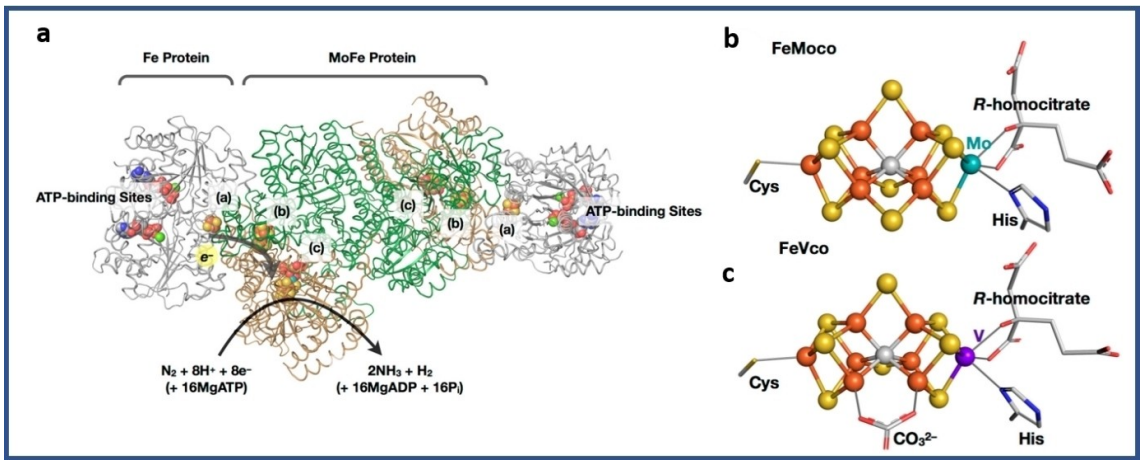

Figure 1. (a) Schematic design of ammonia formation by enzyme nitrogenase along with its protein binding sites and active cofactors. **(b)** and **(c)** chemical structures of FeMo cofactor and FeV cofactor. The structures have been presented through a ball and stick model where colors indicate: blue, N; gray, C; orange, Fe; purple, V; red, O; teal, Mo; yellow, S. Reproduced with permission from Reference [25]. Copyright 2020 American Chemical Society.

several structural and spectroscopic studies where it has been shown that the thermodynamically stable state of nitrogenase is mainly unreactive but dynamical changes with surrounding proteins or local changes in the ligand environment of the FeMo-cofactors might be essential for ambient catalytic reactions.[26] This also includes the breaking of one or more Fe–C/Fe–S bonds.[27–29] Figure 1b and 1c present the chemical structure of such FeMo and VFe cofactors.

3. Photocatalytic N_2 Activation

3.1. History

Photocatalytic nitrogen fixation is a sustainable and green reaction at ambient conditions where solar photons can be directly converted to generate electrons and holes and combine with water protons to reduce N_2 to NH_3. In 1951, the first photocatalytic N_2 activation was reported by Dhar et al. where different sand soils including TiO_2 used to reduce N_2 to obtain a detectable amount of NH_3.[30] In 1955, Eschena and coworkers

Biswajit Bhattacharyya is presently working as a post-doctoral fellow funded by CRC 1636 at the Institute of Chemistry, University of Potsdam. He obtained his Ph.D. from the Indian Institute of Science, Bangalore, in 2018. His research interests include sustainable materials chemistry and photochemical activation for renewable energy applications.

Radwan M. Sarhan received an Erasmus Mundus scholarship and finished his Master's within the SERP CHEM program in 2014. In 2019, he received his PhD under the supervision of Prof. Matias Bargheer at the University of Potsdam, Germany. Since then, he joined the group of Prof. Yan Lu at Helmholtz Centre for Materials and Energy, Germany. His research interests centered around plasmonic catalysis, synthesis of plasmonic-based catalysts, and surface-enhanced Raman spectroscopy.

Yan Lu received her PhD in 2005 with summa cum laude under the supervision of Prof. H.-J. P. Adler at Dresden University of Technology, Germany. After that, she worked first as a postdoc and then research scientist in Prof. Matthias Ballauff's group at the University of Bayreuth. Since 2009, she joined Helmholtz-Zentrum Berlin für Materialien and Energie (HZB) as a group leader in Colloid Chemistry. She was selected as top female researchers (W2/W3-Programme) in Helmholtz Association in 2015. Since 2017, she has been a professor at the Institute of Chemistry at the University of Potsdam. Since 2019, she has been the head of the Department for Electrochemical Energy Storage at HZB.

Andreas Taubert is a professor of supramolecular chemistry and materials chemistry at the University of Potsdam. Previous stations include the University of Basel, the Max Planck Institute for Polymer Research, the University of Michigan, the University of Pennsylvania, and the Max Planck Institute of Colloids and Interfaces. Research interests include materials chemistry in and with ionic liquids, inorganic and hybrid energy materials, and materials for water remediation.

also observed similar reduction reactions. Despite the fundamental interest, these studies did not attract much attention. In 1977, Schrauzer and Guth concluded that nitrogen (N_2) could be reduced to ammonia by iron oxide doped TiO_2 under ultraviolet radiation.[31] In 1983, Schrauzer and coworkers reported again how natural sand has been utilized for N_2 activation.[32] Following these articles, several reports of photocatalytic N_2 activation have appeared. Most notably, the last 10 years have seen substantial progress in this field of research due to the impact of climate change illustrating the need to significantly reduce the carbon footprint.[33–38]

3.2. Basic Mechanism for Photocatalytic N_2 Activation

The basic mechanism of a photocatalytic reaction has three steps. Step one is photon absorption and the creation of excitons or free electrons. Step two is charge carrier separation and migration to the reaction site which is crucial for overall efficiency and the final step is the desired photoreduction or oxidation. Whenever the energy of irradiated light is greater than or equal to the band gap of the absorber, the aforementioned processes happen consecutively. It must be noted that the general mechanism of photocatalytic reactions like H_2 evolution,[39–41] CO_2 reduction,[42–45] or N_2 fixation looks very similar but due to different energy band positions, electron transfer mechanism, and surface binding activities of the catalyst, these reaction mechanisms are completely different and the efficiencies vary drastically. For example, many CO_2 reduction and N_2 activation reactions follow a competitive pathway with H_2 evolution reactions due to similar energy band positions.[46,47]

To design an ideal material for photocatalytic N_2 reductions two things are very important.

(1) Under the irradiation of visible photons, the generated valence band holes can oxidize water [Equation 2], and conduction band electrons will reduce nitrogen [Equation 3]. The overall reaction is the formation of NH_3 and oxygen [Equation 4].[48] NHE signifies the normal hydrogen electrode.

$$\text{Oxidation}: \ 2H_2O + 4h^+ = O_2 + 4H^+ \ (1.23\ \text{V vs. NHE}) \quad (2)$$

$$\text{Reduction}: \ N_2 + 6H^+ + 6e^- = 2NH_3 \ (-0.09\ \text{V vs NHE}) \quad (3)$$

$$\text{Overall reaction}: \ \frac{1}{2}N_2 + \frac{3}{2}H_2O = NH_3 + \frac{3}{4}O_2 \ (\Delta G^0 = 339kJ/mol^{-1}) \quad (4)$$

(2) The catalyst should have significant adsorption capacities for N_2 molecules and favor the desorption of NH_3 or reduced products.

In principle, there are many materials for photocatalytic nitrogen fixation with an ideal band gap close to 2.0 eV where the position of the conduction band is just below the overpotential of N_2 (−0.092 V vs. NHE) and the valence band position is greater than the oxidation potential of water (1.23 V vs. NHE) (Figure 2). But the major challenge is the dissociation/association of N_2 with surface atoms which is the rate-determining step of the reaction.[48,49]

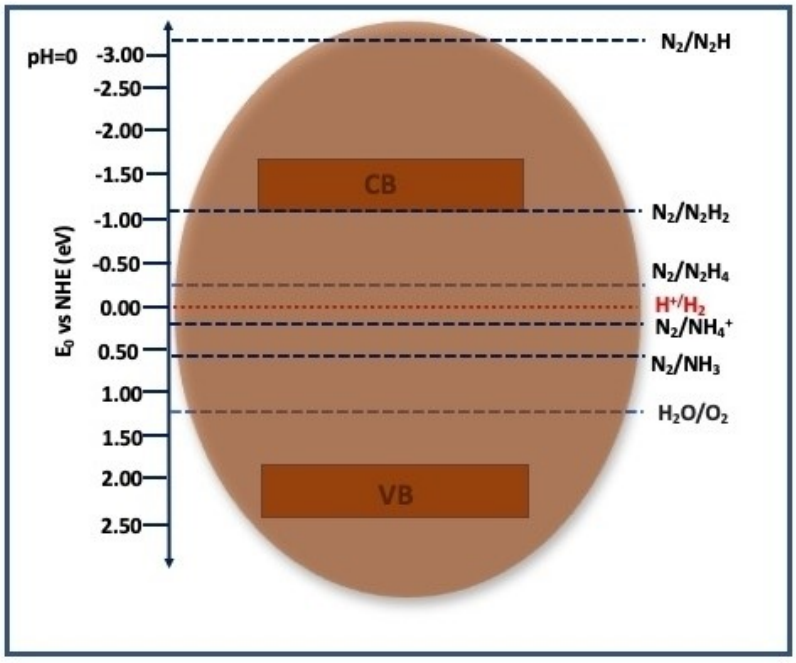

Figure 2. Schematic band diagram of a photocatalytic nitrogen activation reaction.

4. N_2 Binding Mechanism

The binding mechanism of nitrogen follows several steps. Interestingly whether the reaction is governed through the electrocatalytic/photocatalytic pathway, it follows a similar binding mechanism with the surface of the catalyst. For a heterogeneous catalytic mechanism, there are three important steps: (1) chemisorption of N_2 and hydrogen (either as a radical or atom) on the surface of the catalyst, (2) addition of the hydrogen with N_2 atoms in a surface-bound state, (3) consecutive addition of reductive hydrogen and formation of hydrazine and ammonia and (4) desorption of ammonia from the surface of the catalyst. Now the above-mentioned path could be carried through in either dissociative or associative pathways.[50–52]

Figure 3 shows an overview of the N_2 activation mechanisms in heterogeneous catalysis. The main difference between these pathways is the cleavage of the N_2 bond. In the dissociative mechanism, the nitrogen molecule binds to the surface of the catalyst and the cleavage of the N_2 triple bond occurs before the addition of the hydrogen atoms. As the N_2 bond is very stable and has very high bond energy, the dissociative pathway always proceeds through a high energy barrier. For example, the Haber-Bosch synthesis requires very high temperature and rigorous reaction conditions because it goes through a dissociative reaction pathway. In comparison, with the associative reduction mechanism, two nitrogen atoms bind to each other on the surface of the catalyst during the hydrogenation. In photocatalysis, the N_2 molecule takes one proton from the surroundings after binding to the catalyst surface and one electron from the catalyst to form a new intermediate. The whole process goes through several intermediate states with alternating and distal pathways for associative N_2 reduction mechanism.

During the alternating pathway, the N atoms of the adsorbed N_2 are sequentially converted to NH_3 upon receiving hydrogen and electrons. The resultant ammonia molecule is desorbed from the surface of the catalyst after breaking the final N–N bond. In the distal mechanism, the hydrogen binds with the distal nitrogen atom. As a result, the distal nitrogen atom does not interact with the catalyst directly and the hydrogenation of N atoms continues until the first ammonia molecule is released. For the associative alternate and distal mechanism, the breaking of the N_2 triple bond is not needed in the primary step. As a result, it does not proceed through any high energy barrier. In general, both photocatalytic and electrocatalytic activation of N_2 go through the associative reaction mechanism pathway, so it is possible to reduce/activate N_2 in ambient conditions.

5. Photocatalytic Materials for NH_3 Synthesis

The basic reaction mechanisms which are all discussed in the previous sections, are quite important for designing new materials for efficient reduction of N_2. In this section, we are going to discuss some well-known materials for photocatalytic N_2 activation where the structural correlations, optical properties, and basic reaction mechanisms have been analyzed.

5.1. Metal Oxides

5.1.1. Oxygen Vacancies and Heteroatom Doping

Various metal oxides have been extensively used for nitrogen reduction reactions (NRR) in both photocatalytic and electrocatalytic processes.[53,54] The first photocatalytic NRR was based on a Fe-doped TiO_2 where TiO_2 was used as a photo absorber

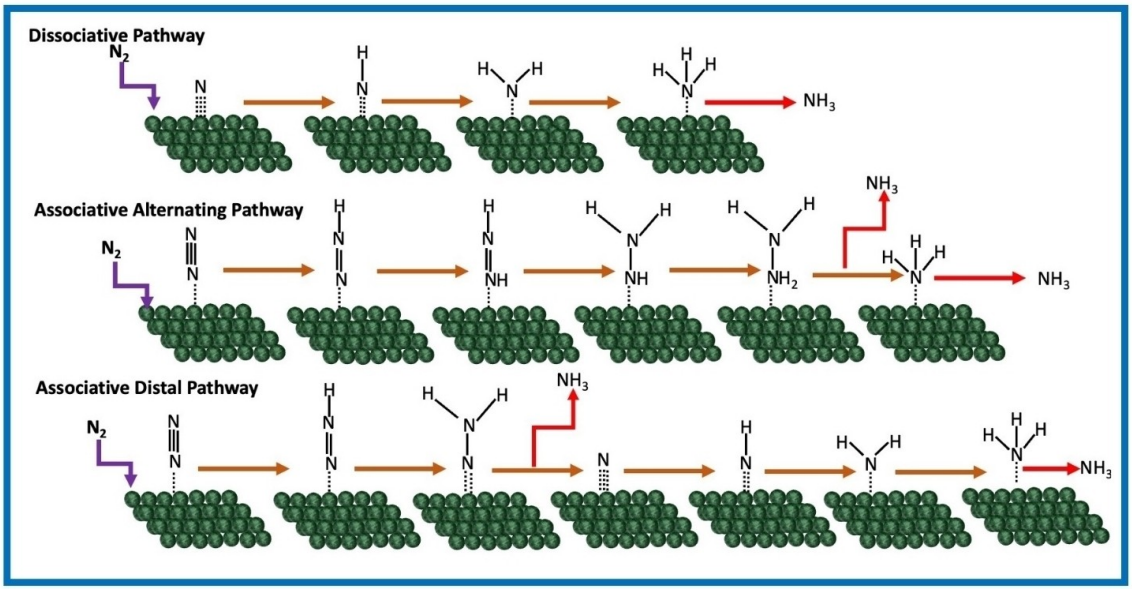

Figure 3. Mechanistic overview of N_2 activation in a heterogeneous catalytic reaction.

and the Fe centers were used an active site for the NRR.[55] TiO_2 is also the most well-known material for photocatalytic H_2 evolution[56] and CO_2 reduction,[57,58] even though, due to the wide band gap, it is not a perfect visible light absorber. Various techniques have been implemented to increase the absorption cross sections of TiO_2 in the visible region. For example, anion doping where TiO_2 was doped with various anions like nitrogen,[59] phosphorus, or halogens[60] to shift the band gap towards the red . But, overall, the photocatalytic efficiencies did not increase drastically due to the poor surface binding property of titanium which is the main step for NRR. Later, various research groups came up with the idea of transition metal (TM) doping like Fe,[61] Ni,[62] Mo,[63] etc. With TM doping the surface binding activity indeed changed but did not improve the overall performance. Clearly, for a catalyst to perform effectively, surface binding of the substrates and strong light absorption should both happen simultaneously. Figure 4a shows the schematic diagram of how adjacent bi-Ti^{3+} pairs form on anatase TiO_2 which act as active centers for N_2 chemisorption and activate photoreduction in the presence of dopants like Zr^{4+}. If we look into the microstructure of these compounds, it is clear that up to 5% of dopant concentration, Zr^{4+} acts as an isolated metal atom on top of the TiO_2 nanotube and does not form any isolated nanoparticle of Zr(Figure 4b).[64] In a similar way same effect has been observed for a Fe-doped TiO_2 whereas dopant Fe decreased the crystallite size and up to 10% in weight, it does not form any nanoparticle or oxide contaminants (Figure 4c). In both cases, the NRR yields improve drastically in the presence of a dopant. For example, Fe-doped TiO_2 shows the overall yield of ammonia formation is 5 times higher than undoped TiO_2 in the first two hours of the reaction (Figure 4d).[65]

Oxygen vacancies (OVs) and heteroatom doping are two widely used approaches to tune the electronic structure of TiO_2 and enhance the NRR performance.[66] Figure 4e gives a brief idea about the N_2 binding in an OV–TiO_2. With the formation of OVs on the surface of TiO_2, the number of unsaturated Ti^{3+} sites increase. This directly enhances the capture and activation of N_2. At the same time to understand the presence of OVs in TiO_2, ESR could be a powerful technique (Figure 4f). With the optimized number of OVs, the bandgap also becomes narrower. Although high numbers of OVs can strengthen the adsorption of N_2 on TiO_2, they also serve as local recombination centers for electrons and holes which can reduce the efficiency of photocatalytic N_2 fixation.[67]

Similarly, the formation of heterostructures from noble metals and semiconductors has enhanced the overall performance of NRR in TiO_2 systems. For example, Liu *et al.* reported a TiO_2@C/g-C_3N_4 type-II heterostructure photocatalyst for NRR, which shows good yield in the NH_3 formation.[68] Under visible light, the electrons excite from the valence to the conduction band of g-C_3N_4. Consequently, electrons are transferred to TiO_2 and holes remain in g-C_3N_4, which prolongs the recombination of charge carriers. As a result, the NRR performance of this

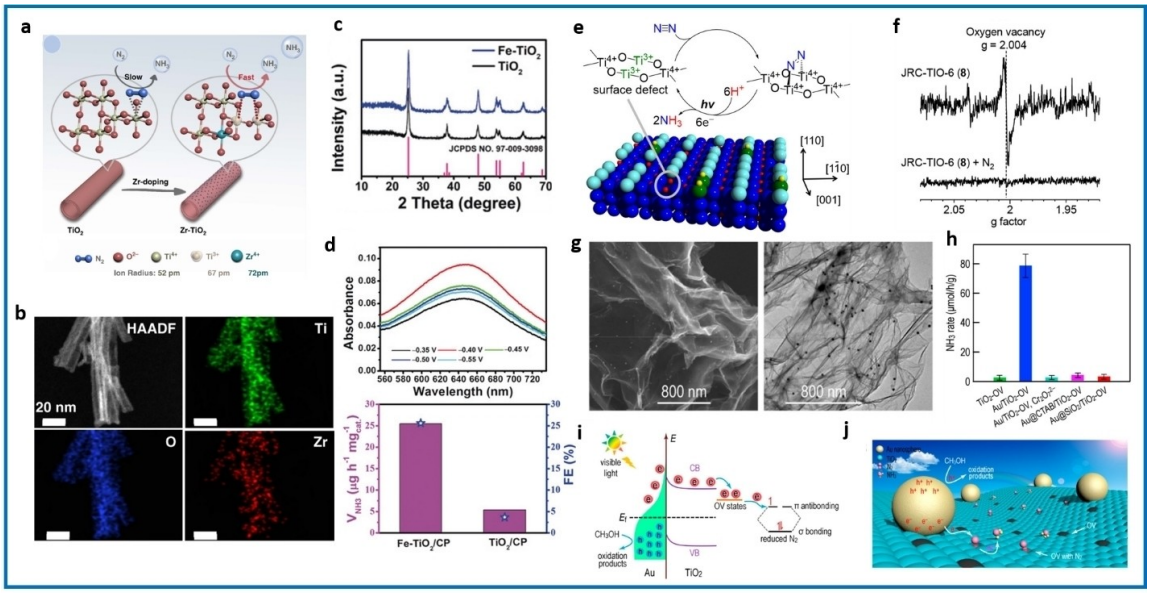

Figure 4. (a) Schematic image of oxygen vacancy with two adjacent Ti^{3+} sites in a Zr-doped anatase TiO_2. **(b)** High-angle annular dark-field scanning transmission electron microscopy (HAADF-STEM) images with corresponding element mapping of a cylindrical hollow Zr–TiO_2 where Ti represents green, O with blue, and Zr represents red. (a, b) Reproduced with permission from Reference [64]. Copyright 2019 Springer Nature. **(c)** XRD pattern of Fe-doped TiO_2 nanostructures. **(d)** UV-visible absorption spectra of the electrolytes in indophenol indicator (top) and quantitative yields of NH_3 formation in both TiO_2 and Fe-doped TiO_2 with corresponding faradic efficiency (bottom). Reproduced with permission from Reference [65]. Copyright 2019 Wiley and Sons. **(e)** Mechanistic overview of NH_3 formation in Rutile TiO_2 (110) surface. **(f)** The Electron Paramagnetic Resonance (EPR) signal of an oxygen-vacant TiO_2. (e, f) Reproduced with permission from Reference [67]. Copyright 2017 American Chemical Society. **(g)** SEM (left) and TEM (right) images of the Au/TiO_2–OV sample. **(h)** The rate of N_2 photo fixation with different catalysts. **(i, j)** Schematic illustration of the plasmonic hot electron generation, injection, and N_2 reduction processes in the surface of Au/TiO_2–OV catalyst under visible light with an artistic view. (g, h, i, and j) Reproduced with permission from Reference [69]. Copyright 2018 American Chemical Society.

heterostructure is about one order of magnitude higher than individual g-C_3N_4 and TiO_2. A similarly efficient NRR has been observed for an Au/TiO_2–OV catalyst. Figure 4g shows the typical electron microscopic images of the catalyst where Au nanoparticles have been anchored into TiO_2–OV nanosheets. Figure 4h compares the rate of NH_3 formation in different conditions. The Au/TiO_2–OV catalyst shows almost an order of magnitude higher yields compared to TiO_2–OV catalysts. It is quite clear that this plasmonic N_2 photo fixation mechanism goes through several steps and the most important step is the activation of N_2 molecules at the OV sites. Later the injection of hot electrons from Au nanospheres into the conduction band of the TiO_2 nanosheets and trapping of the injected hot electrons by the OV-induced defect states happen consecutively. Finally, the reduction of the activated N_2 molecules by the hot electron occurs at the OV sites (Figure 4i and 4j).[69]

5.1.2. Bismuth Oxyhalides and Metal Substituted Bismuth Oxides

The photocatalytic applications of bismuth-based materials have drastically increased over the last few years. Ease of synthesis, environmental stability, and low toxicity are the main three advantages of these materials. Recent observations have shown that bismuth-based oxides,[53] sulfides,[70] and halides are rather poor materials for the hydrogen evolution reaction (HER) which can indirectly boost nitrogen fixation with proper band structure and binding activities.[71]

Among all bismuth-based compounds, bismuth-based oxyhalides have been known for photocatalytic application for quite some time.[72] For example, $Bi_4O_5Br_2$, $Bi_{24}O_{31}Br_{10}$, and Bi_3O_4Br have extensively been used for dye degradation, water splitting, and CO_2 reductions.[73–76] In general, with an increasing Bi/Br ratio there is an effective increase of optical absorption and enhancement of photostability. In 2017 Wang et al. reported the first ultrafine Bi_5O_7Br nanotubes for photocatalytic N_2 fixation where water was the hydrogen source.[77] They have explained the mechanistic overview of the photocatalytic NRR. It has been also proved that oxygen vacancies (OVs) can enhance the catalytic reactions for this class of materials. Figure 5a–c shows the typical schematic structures (both top and side view) and transmission electron microscope (TEM) images of Bi_5O_7Br nanotubes. Figure 5d–e shows the different rates of NH_3 formation with various structural morphology and isotope-labelled NMR data of product formations.

Besides the oxobromides, similar observations have been proved for chloride-based materials like BiOCl. Zhang et al. have reported OV-enriched Fe-doped BiOCl nanosheets for photocatalytic nitrogen fixation.[78] Figure 5f–g shows TEM and AFM images of these nanosheets synthesized through hydrothermal reaction. BiOCl nanosheets with 5% Fe doping (BiOCl NSs–Fe–5%) showed an exceptional photocatalytic N_2 fixation performance rate of NH_3 formation (1.022 mmol h^{-1} g^{-1}) and turnover frequency (TOF) of 0.863 h^{-1}. The material also shows an apparent quantum efficiency (AQE) of 1.8% at 420 nm with good durability as a photocatalyst (Figure 5h–i). Alternatively, the metals substituted bismuth oxides are also well known for photocatalytic NRR. Meng et al. have shown that Fe-doped Bi_2MoO_6 could be an efficient photocatalyst for N_2 fixation.[79] Very recently bismuth monoxide-based quantum dots have been studied for photocatalytic reduction of N_2 to ammonia with very good yields. 2–5 nm size particle of BiO can produce

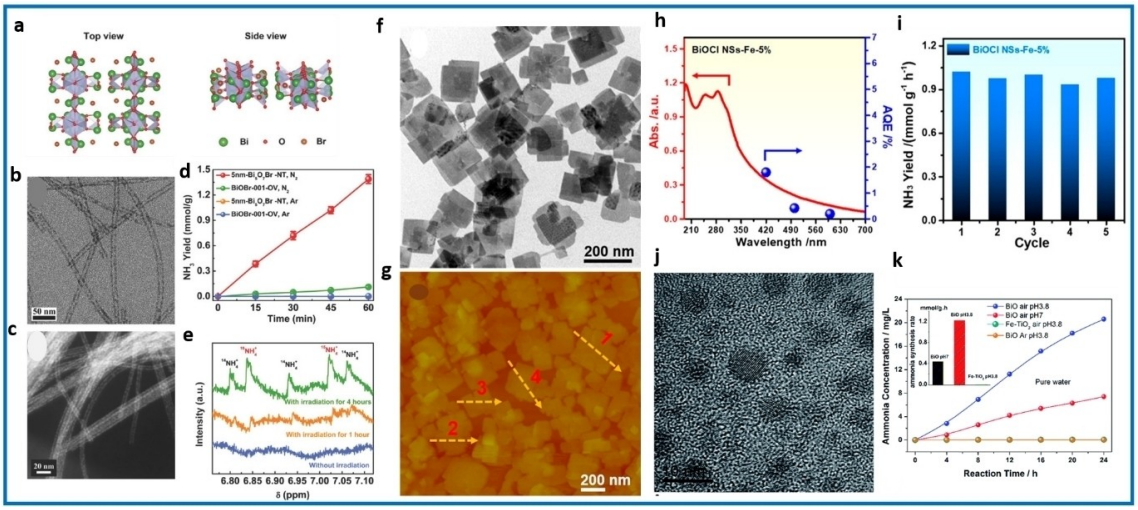

Figure 5. **(a)** Crystal structure of Bi_5O_7Br nanotubes. **(b)** TEM images of Bi_5O_7Br nanotubes. **(c)** STEM images of Bi_5O_7Br nanotubes. **(d–e)** Quantitative yields of NH_3 formation and proton NMR (400 MHz) spectra as a function of time using 50 vol% $^{15}N_2$ as the N source. (a–e) Reproduced with permission from Reference [77]. Copyright 2017 Wiley. **(f–g)** TEM and AFM images of BiOCl NSs–Fe–5% where line 1–4 denote the height profile of the sample. **(h)** Calculated Apparent Quantum Efficiency (AQEs) (blue dots) for N_2 fixation over BiOCl NSs–Fe-5% in pure H_2O under monochromatic light irradiation along with material UV-visible absorption spectra (red-line). **(i)** Photocatalytic stability tests for BiOCl NSs–Fe–5%. (f–i) Reproduced with permission from Reference [78]. Copyright 2019 American Chemical Society. **(j)** HRTEM images of BiO quantum dots. **(k)** Photocatalytic N_2 reduction performance of the as-prepared BiO quantum dots under different reaction conditions with simulated solar light irradiation. (j–k) Reproduced with permission from Reference [80]. Copyright 2016 Royal Society of Chemistry.

ammonia 1000 times higher amount than traditional photocatalysts like Fe-doped TiO_2 (Figure 5j–k).[80]

Low valent metal oxide especially bismuth-oxide plays a crucial role in N_2 activation due to higher affinity towards the binding of the N_2 molecule.[81] N_2 bonding can be achieved through donating electrons and back bonding with empty 6p orbitals of bismuth atoms. Once these metal atoms or ions bridge with the N_2 bond through the transfer of the electron to N_2 antibonding orbitals, the N≡N triple bond is weakened significantly. Similar observations have been proved for vacant d orbital of transition metals and empty p orbitals for alkaline earth metals.[82,83,84]

5.2. Metal Sulfides

Compared to metal oxides, metal sulfides are not very well investigated as photocatalytic materials for NRRs. Due to the strong affinity towards H_2 evolution, binding of hydrogen atoms with the N_2 in the transition states is not feasible thermodynamically.[85,86] As a result, the consecutive steps of NRRs are quite difficult to realize and typically do not occur. Still, some metal sulfide-based materials are emerging as photocatalytic materials with various 2D confined structures, especially transition metal dichalcogenides.[87–91] In 2021 Chen et al. reported $Bi_2S_3/KTa_{0.75}Nb_{0.25}O_3$ nanocomposite for photocatalytic and piezo catalytic NRRs.[92] Figure 6a shows the band structure of $KTa_{0.75}Nb_{0.25}O_3$(KTN)/Bi_2S_3 heterostructures and Figure 6b shows the transient photocurrent response of the composite. All materials exhibit stable and reversible photocurrent response with light on/light off cycle and it is quite clear that Bi_2S_3 greatly enhances the charge separation efficiency of KTN under simulated sunlight. Qin et al. have observed a similar effect for $AgInS_2$, a ternary sulfide quantum dot with 2D-MXene where it forms a 0D/2D heterostructure. $AgInS_2$ acts as a photo absorber but the NRR reaction takes place on the active site of MXene.[93] MoS_2 monolayers have been also reported for photocatalytic N_2 activation to ammonia with high yields.[94] The multiexciton generation after photo absorption helps to achieve the consorted kinetically favored path for NH_3 production. In 2020, Sun et al. reported sulfur vacant-O rich 1T-MoS_2 nanosheets which show superior performance than Pt as a cocatalyst with CdS nanorods for the photocatalytic nitrogen fixation.[95] O-doped sulfur vacant MoS_2 metallic nanosheets (Figure 6c) were deposited on top of CdS nanorods (Figure 6d). The heterostructure forms a band offset which acts as a photochemical activator for N_2 reduction (Figure 6e). As a result, the material 30 wt% SV-1T-MoS_2/CdS shows phenomenal performance under simulated solar light irradiation where chemical yields go to almost 8000 $\mu molh^{-1}g^{-1}$ (Figure 6f). Unfortunately, however, in the presence of visible light, the catalytic performance is not satisfactory compared to simulated solar light (Figure 6g).

5.3. Plasmonic Materials

Plasmonic metal nanoparticles, such as Au, Ag, and Cu, strongly interact and harvest light, thanks to their localized surface plasmon (LSP). Optical excitation of these particles causes

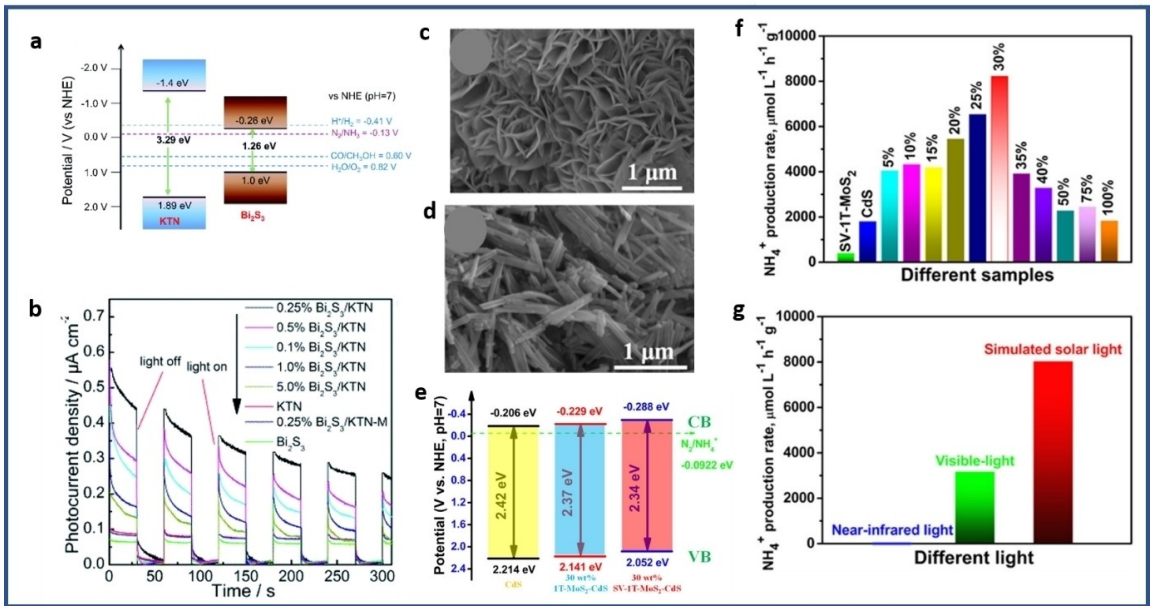

Figure 6. (a) Schematic band diagram of photocatalytic and piezocatalytic N_2 fixation in the Bi_2S_3/KTN composite structure. **(b)** Transient photocurrent response of KTN, Bi_2S_3, and Bi_2S_3/KTN photocatalysts. (a–b) Reproduced with permission from Reference [92]. Copyright 2021 Royal Society of Chemistry. **(c–d)** SEM images of sulfur vacant 1T-MoS_2 and CdS nanorods. **(e)** Band structure of CdS, 30 wt% 1T-MoS_2/CdS, and 30 wt% SV-1T-MoS_2/CdS composites. **(f)** Photocatalytic NH_4^+ production rates for SV-1T-MoS_2, CdS nanorods, and SV-1T-MoS_2/CdS composites containing different amounts of cocatalysts (5, 10, 15, 20, 25, 30, 35, 40, 50, 75, and 100 wt%) under simulated solar light irradiation. **(g)** photocatalytic NH_4^+ production rates of 30 wt% SV-1T-MoS_2/CdS composites under different light irradiation. (c–g) Reproduced with permission from Reference [95]. Copyright 2020 American Chemical Society.

collective oscillations of the free electrons, which generates the surface plasmon in the visible and near-infrared ranges of the solar spectrum, which is responsible for their bright colors. The surface plasmon works as a mediator to redistribute and convert photon energy into electronic and thermal energies, which are utilized to drive chemical transformations of the adsorbed molecules, known as plasmonic chemistry.[96,97] Plasmon-induced catalytic reaction, driven by light, has become a promising and alternative strategy to conventional thermochemistry, thereby driving chemical reactions under considerably mild conditions on plasmonic metal catalysts.[98,99] Upon the LSP excitation, energetic charge carriers (hot electrons and holes) and a high local temperature (photothermal effect) are generated, which offers new channels for driving chemical reactions via injection of the hot charge carriers into the molecular orbital of the reacting molecules. Herein, the strong heating effect can be used to overcome the activation barrier of the chemical reaction.[100–107] Particularly, the hot electrons, which have shown to be effective for many chemical reactions, have been also utilized for NRRs at room temperature as an alternative pathway of the common Haber–Bosch process that requires high temperatures.[108–110]

In the plasmon-enhanced NRR experiments, the plasmonic-based catalysts have been commonly used in two configurations: plasmonic metal-semiconductor and metal-metal hybrid structures.[111] In the former structures, plasmonic metal nanoparticles, such as Au, are used to generate hot electrons as well as to broaden the absorption of the semiconductor, while the semiconductor acts as the catalytic center and is further utilized to inhibit the hot electron-hole recombination by the Schottky barrier formed in the process. Thangamuthu and co-workers have developed a photocatalyst using plasmonic aluminum nanotriangles (AlNTs) as a cheaper and more abundant alternative to the expensive gold particles, forming an AlNTs–TiO_2 hybrid substrate.[112] Upon light illumination (at 365 nm) a quantum efficiency of ~0.025% and 0.06% were estimated for the bare TiO_2 and AlNTs–TiO_2, respectively. This shows that the ammonia production was enhanced by a factor of 2.4 after the incorporation of the plasmonic particles, which confirms the role of the hot electrons for NRR. In 2019, Jia and co-workers have shown that gold nanorods tipped with ceria (Au/end-CeO_2) can work as an excellent catalyst for plasmon-induced photo fixation of N_2 under near-infrared irradiation (808 nm).[113]

In the second catalyst configuration, the plasmonic metal is combined with another transition metal that works as a binding site and catalytic center for the N_2 molecules. The hot electrons generated from the plasmonic particles are allowed to flow to the non-plasmonic particles, and thus enhance the reaction rate. In this sense, Zeng and co-workers have prepared Os–Au composite nanoparticles for ammonia synthesis at ambient conditions under visible light irradiation.[114] The authors showed that the NH_3 production rate follow the same pattern as the plasmon band of Os–Au particles, which were attributed to the flow of the plasmon energy from Au to Os particles upon resonant excitations. In 2019 Hu et al. reported AuRu-based core-antenna nanostructures (Figure 7a–b) for efficient photocatalytic NRRs with various stoichiometry of Au and Ru (Figure 7c).[115] The particles exhibit a morphology of plasmonic Au core and catalytic AuRu alloy antennas and the NRR experiments are conducted under a broadband light illumination. The particles alloyed with a 31% molar ratio of Ru display the highest NH_3 production rate, while higher Ru contents (more than 40%) decrease the production rate as the light-harvesting capability of the particles is significantly reduced. The authors assign the enhancement of the catalytic performance to the strong local electric field together with the flow of the hot electron from Au to Ru and direct excitation at the catalyst–N_2 interface (Figure 7d–f). In 2020, Hou et al. have successfully prepared low-cost Cu-based photocatalysts for plasmon-assisted N_2 photofixation.[116] The catalyst comprises surface Fe atoms as the active sites for the N_2, and Cu frameworks as the plasmonic compartments, forming porous CuFe of various stoichiometries. The NRR experiments were conducted under broadband irradiation (320–780 nm, Xe lamp, 250 mW/cm^2). The authors have shown that porous $Cu_{96}Fe_4$ displayed an NH_3 production rate of 342 $\mu mol g_{cat}^{-1} h^{-1}$ without any sacrificial agent in addition to its excellent stability for 10 cycles. In 2017 Carter et al. showed theoretically how Mo-embedded Au nanoparticles can enhance the rate of photocatalytic NRRs (Figure 7g).[117] The Au portions act as a light-harvesting antenna and transfer the energy onto the Mo active site through tunneling where excited states are generated in the near-infrared–to–visible plasmon regime. The activation energy of N_2 reduction effectively lowers from 3.5 eV (335 KJ/mol) to 0.44 eV/N_2 (43 kJ/mol) in the ground state. The overall reactivity is enhanced through surface resonance energy transfer due to the plasmon local field (Figure 7h).

5.4. MXenes

Two-dimensional (2D) transition metal carbides, nitrides, and carbonitrides (MXene) are becoming very popular catalytic materials for CO_2 reduction, H_2 evolution, NRR, and wastewater treatments. The layer morphology with the exposed surface edges of the MXenes plays a critical role in these applications.[118] For example, Wang et al. have reported that $Ti_3C_2T_x$ nanosheets show high faradic efficiency (5.78%) for NH_3 electrosynthesis with ultralow potential.[119] On a similar note, these materials have different activation barriers for the basal plane and the edge plane. As a result, there are different rates of formation for NRR reactions. Figure 8a gives a brief idea of how the activation of energy for the N_2 bond. Even activation energy varies for different functionalized basal planes. Johnson et al. have theoretically explored the active site of MXenes for electrocatalytic NRRs. Considering the active basal plane of these materials, the effect of transition metals (Mo, W, V, etc.) and other anions (O, F, S, Cl) on electrocatalytic NRRs have been calculated (Figure 8b). The calculated free energy diagram gives an idea of how the intermediate steps of N_2 activation vary with differently terminated MXenes $Ti_3C_2T_x$ and Ti_2CT_x with T_x = bare, H, O, and N.[120]

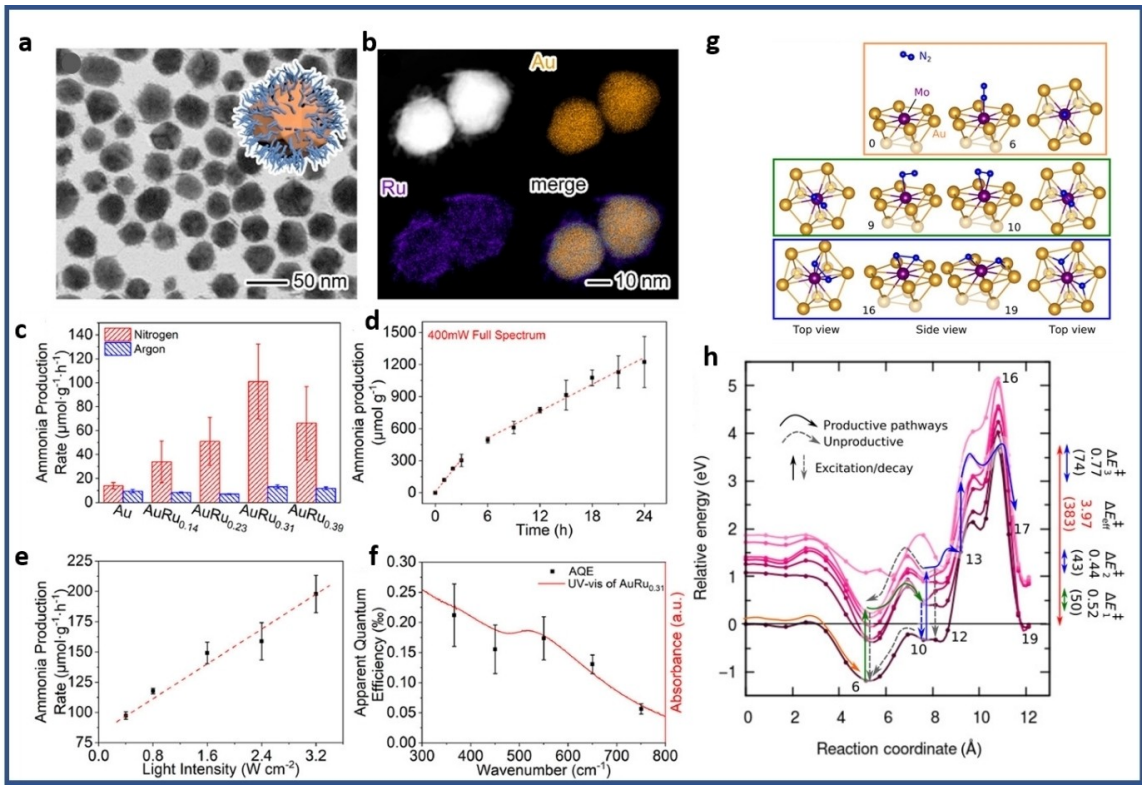

Figure 7. (a) TEM image of $AuRu_{0.31}$ core-antenna nanostructures. **(b)** Corresponding Energy-dispersive X-ray spectroscopy (EDS) elemental mapping profiles of $AuRu_{0.31}$ nanostructure showing the elemental distribution of Au (orange) and Ru (purple). **(c)** Photocatalytic ammonia production rates for the first 2 hours with different stoichiometry of Ru bare Au, $AuRu_{0.14}$, $AuRu_{0.23}$, $AuRu_{0.31}$, and $AuRu_{0.39}$ **(d)** Time-dependent photocatalytic ammonia production by $AuRu_{0.31}$ in 24 h in similar reaction conditions. **(e)** Photocatalytic ammonia production rates by $AuRu_{0.31}$ in the first 2 h under different light intensities. **(f)** Calculated AQEs for N_2 fixation over $AuRu_{0.31}$ in pure water under 20 mW cm^{-2} monochromatic light irradiation, with its UV–vis extinction spectrum (red line) as a reference. (a–f) Reproduced with permission from Reference [115]. Copyright 2019 American Chemical Society. **(g)** DFT–predicted stationary and transition-state structures of Mo-doped Au (111) surface for N_2 dissociation. **(h)** Ground and excited state energy curve for the excited state. Possible lower activation energy barriers are marked with arrows. Ground and excited state effective thermal barriers are shown on the right margin (in eV and kJ/mol). (g–h) Reproduced with permission from Reference [117]. Copyright 2017 American Association for the Advancement of Science.

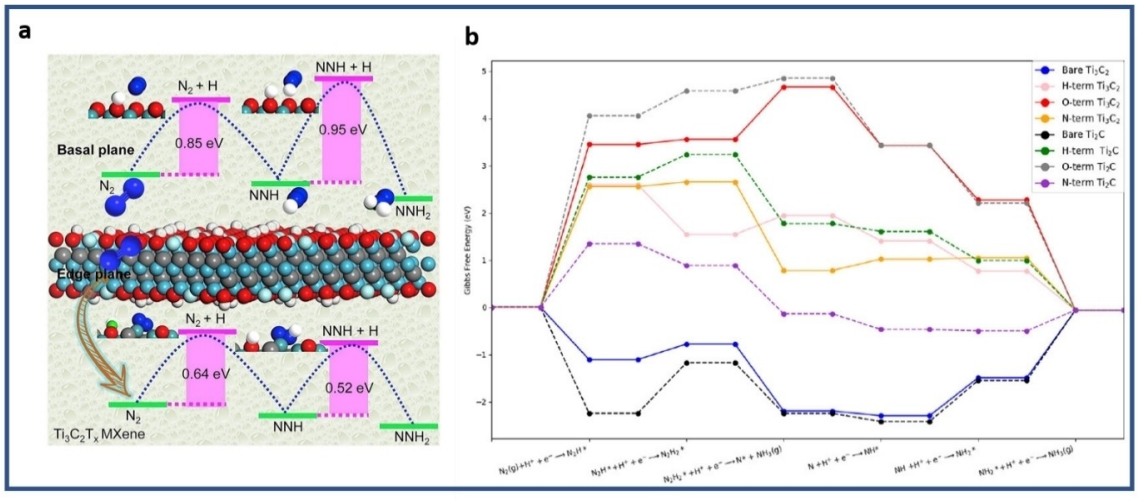

Figure 8. (a) Comparison of N_2 activation barriers on the basal plane and the edge plane of $Ti_3C_2T_x$ MXene. Reproduced with permission from Reference [119]. Copyright 2019 Cell Press. **(b)** Calculated free energy diagrams for the proposed associative NRR mechanism on $Ti_3C_2T_x$ where T_x = bare, H, O, and N. Reproduced with permission from Reference [120]. Copyright 2020 American Chemical Society.

There are also various reports on experimental electrocatalytic NRR with Ti-based MXenes[121,122] but photocatalytic approaches are largely unexplored. Only very recently a few studies on MXene-based heterostructures for photocatalytic

NRRs have appeared. Chang et al. have reported a sandwich structure made of Ti_3C_2 and Au nanosphere where Au nanospheres act as a photocatalyst and layered Ti_3C_2 for N_2 activation in pure water under ambient conditions.[123] Different morphologies of layered r-Ti_3C_2/edge-Au hybrids, especially the different loading of Au nanoparticles have been analyzed for enhancement of reaction rates. Partially reduced layered Ti_3C_2 MXene with exposed low-valence Ti sites act as active sites for capturing and activating N_2 molecules. Embedded Au nanospheres transfer plasmonic hot electrons to reduce the activated N_2. Most importantly, the unique sandwich-like architecture of layered r-Ti_3C_2/edge-Au prevents the self-stacking of the Ti_3C_2 layers and directly favors the exposure of the active sites for N_2 activation (Figure 9a). Fang et al. have reported similar observations for BiOBr/Ti_3C_2-based structures.[124] The material creates double vacancies such as oxygen in BiOBr and titanium in Ti_3C_2 composites which creates local sites for N_2 binding. The microscopic picture depicts the oxygen vacancy and heterostructure with the very clear interface of BiOBr/Ti_3C_2 (Figure 9b–c). Upon excitation with visible photons, the material can efficiently reduce N_2 to NH_3 through interfacial electron transfer (Figure 9d–e).

5.5. Metal Free Catalysts

Graphitic-carbon nitride (C_3N_4) is a well-known metal-free photocatalyst for various catalytic reactions.[125,126] In this regard, both the pristine and doped g-C_3N_4 have been applied in electrocatalytic NRR.[127,128] The material is gaining much attention due to weak hydrogen adsorption and evolution performance. Besides that, these materials act as Lewis acid sites which can accept the lone-pair electron of N_2 and bind N_2 simultaneously with its electron-deficient centers. Alternatively, it can also act as a perfect photocatalytic material due to its band gap of 2.7 eV. Although the bulk material is not suitable due to low porosity and low number of active sites, by proper surface functionalization, the catalytic activities can be drastically enhanced. In 2018, Ling et al. have shown theoretically how boron (B) decorated optically active B/g-C_3N_4 could be an efficient photocatalytic material for NRR.[38] B decoration effectively enhances the optical absorption of the pristine C_3N_4 significantly in the visible range (Figure 10a). At the same time, B decoration does not break the g-C_3N_4 framework (Figure 10b). Charge density calculation reveals that there is significant charge transfer between the anchored B atom and N_2 molecule (Figure 10c) and free energy calculations explain the further reaction mechanism of NH_3 formation. Similar observations have been made by Zheng et al. who showed that boron atom decorated poly (triazine imide) (B/PTI), a crystalline carbon nitride, is an excellent thermal catalyst for nitrogen activation (Figure 10d–e). They have also proposed a substrate-hydrogen binding mechanism with less activation barrier of hydrogen migration in the transition state.[129] In 2015, Dong et al. reported how the nitrogen vacancies (NVs) in graphitic carbon nitride (g-C_3N_4) can enhance the photocatalytic N_2 fixation ability (Figure 10f).[130] In 2020, Wang et al. have shown experimentally that B–C-N networks enhance the photocatalytic NRR activities in B-doped C_3N_4.[131]

Frustrated Lewis pairs (FLPs), consisting of sterically hindered Lewis acids and bases, are highly reactive systems capable of activating dinitrogen (N_2). It worked cooperatively to weaken and split the N≡N triple bond. Recent advances include the use of borylene and phosphine FLPs and transition metal-

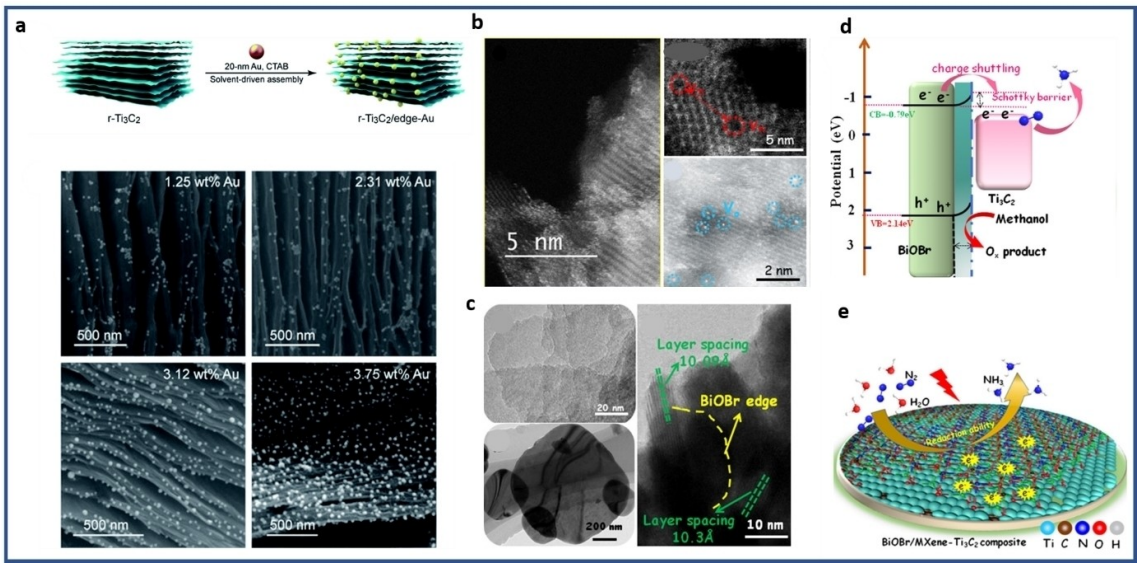

Figure 9. (a) Schematic illustration of the synthesis process of layered r-Ti_3C_2/edge-Au and SEM images of r-Ti_3C_2/edge-Au with different loads of Au. Reproduced with permission from Reference [123]. Copyright 2021 Royal Society of Chemistry. **(b)** Aberration-corrected HAADF-STEM image of 10 wt% BiOBr/Ti_3C_2. **(c)** HRTEM image of layered MXene (Ti_3C_2) nanosheets, BiOBr flakes, and 10% BiOBr/Ti_3C_2 (the green dashed line represents the layer spacing of Ti_3C_2; the yellow dashed line is at the interface between materials). **(d–e)** The relative position of the energy band of the material and the space charge separation and transport scheme in the photocatalytic N_2 reduction process on the BiOBr/Ti_3C_2 composite material. (b–e) Reproduced with permission from Reference [124]. Copyright 2021 American Chemical Society.

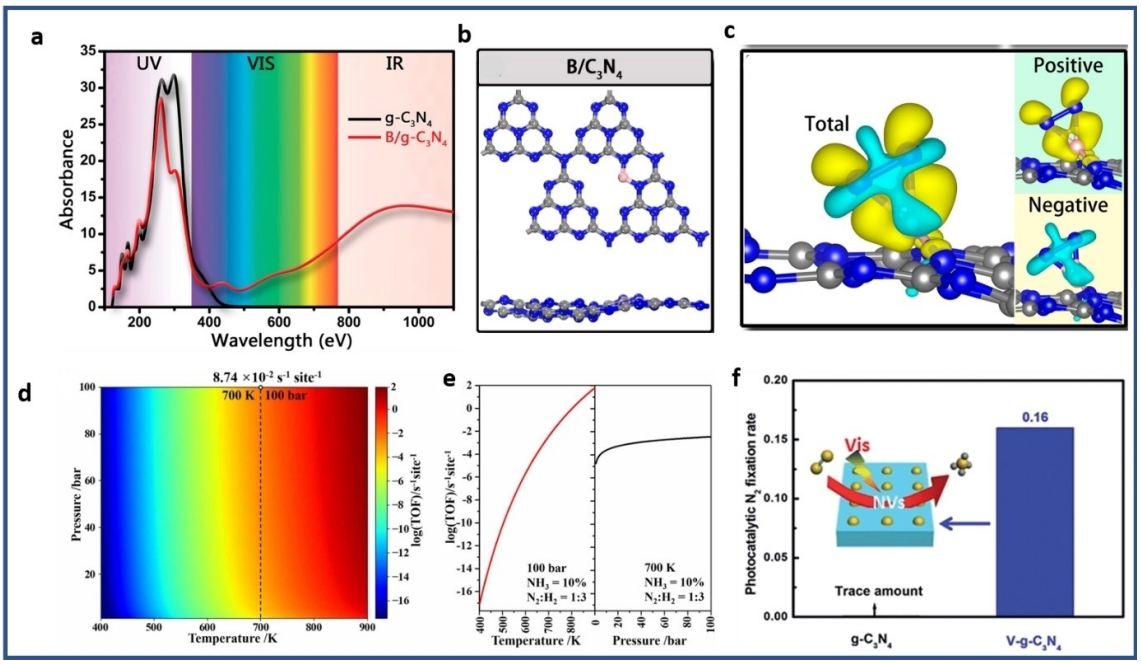

Figure 10. **(a)** Optical adsorption spectra of pure g-C_3N_4 and B/g-C_3N_4, which are illustrated by the black and red lines, respectively. **(b)** Top and side structural views of B/g-C_3N_4. **(c)** Corresponding N_2 adsorption with electron density distribution. (a–c) Reproduced with permission from Reference [38]. Copyright American Chemical Society. **(d)** Turnover frequency (TOF) for ammonia synthesis over B/PTI at different temperatures and pressures with the partial pressure of N_2:H_2 = 1:3. **(e)** Plots of TOF at various temperatures at 100 bar (left) and various pressures at 700 K (right) for the same systems. Reproduced with permission from Reference [129]. Copyright 2022 IOP publishing. **(f)** Photocatalytic N_2 fixation rate of g-C_3N_4 and V-g-C_3N_4. Reproduced with permission from Reference [130]. Copyright 2015 Royal Society of Chemistry.

free systems like $B(C_6F_5)_3$ with tBu_3P, showing promise under mild conditions. Despite challenges in selectivity, efficiency, and scalability there is tremendous progress in FLP properties and deepening mechanistic understanding for practical applications in sustainable nitrogen activation.[83–85,89]

In summary, while there are numerous theoretical studies, which claim a substantial improvement in metal-free catalysts for photocatalytic NRR, the number of experimental studies is still very limited.[132] At the same time, there is a chance for N contamination in these types of materials. So, the isotope label experiment with proper quantification of reduced product is very important.

5.6. Biomimetic Catalysts

Nitrogenase is a complex enzyme found in nitrogen-fixing bacteria that can activate N_2 and convert it into ammonia (NH_3) at ambient conditions. The active site of nitrogenase contains an iron-sulfur cluster, which coordinates with N_2 and activates it for further chemical reduction.[133,134] In this regard, biomimicry can be a powerful way to find inspiration for new catalysts that can activate N_2 more efficiently and sustainably.

Among the various possible biomimetic approaches, a particularly promising one is to mimic the active site of the nitrogenase enzyme, which is mainly found in nitrogen-fixing bacteria and is capable of converting N_2 into ammonia (NH_3). The synthetic catalysts will mimic the active site, using iron, molybdenum, and other transition metals. In recent years, researchers have made significant progress in developing new biomimetic catalysts for N_2 activation. For example, in 2015 Banerjee et al. proposed FeMoS-chalcogels for efficient photochemical conversion of N_2 to ammonia.[135] The chalcogels are made of $[Mo_2Fe_6S_8(SPh)_3]^{3+}$ and $[Sn_2S_6]^{4-}$ clusters which have strong optical absorption, enhanced surface area, and good aqueous stability in their solution phase (Figure 11a–b). Despite this, the yield of NH_3 formation was low and needed a very high catalyst loading. In 2020 Zheng et al. reported nitrogenase enzyme-inspired inorganic chalcogenide compounds for the efficient electrochemical conversion of N_2 to NH_3.[136] The basic motif of structure was 2D single-layered MoS_2 ($sMoS_2$) with [Fe–S_2–Mo] referred as Fe–$sMoS_2$. The microstructure explains the atomic substitution of Fe atom in the layered structure of MoS_2 at Mo site and at the same time there is a creation of S vacancy due to excess Fe atoms (Figure 11c). The material shows a high activity of 8.7 mg_{NH3} mg_{Fe}^{-1} h^{-1} (24 μg_{NH3} cm^{-2} h^{-1}) with an excellent faradaic efficiency of 27% for the conversion of N_2 to NH_3 in aqueous medium. Recently, the same authors have shown photocatalytic conversion of ammonia at elevated temperatures using similar Fe–S_2–Mo bioinspired inorganic structures. The solar-to-NH_3 energy conversion efficiency can be up to 0.24% at 270 °C, which is the highest efficiency among all reported photocatalytic systems and also shows the high-temperature stability of the catalyst.[137] Heat promotes the longer photon-induced exciton lifetime and also enhances the catalytic activity (Figure 11d). The Bader charge distribution of the corresponding atoms in Fe–$sMoS_2$ and Fe_3S_4 explain the basic multipole moments of different atoms which have very

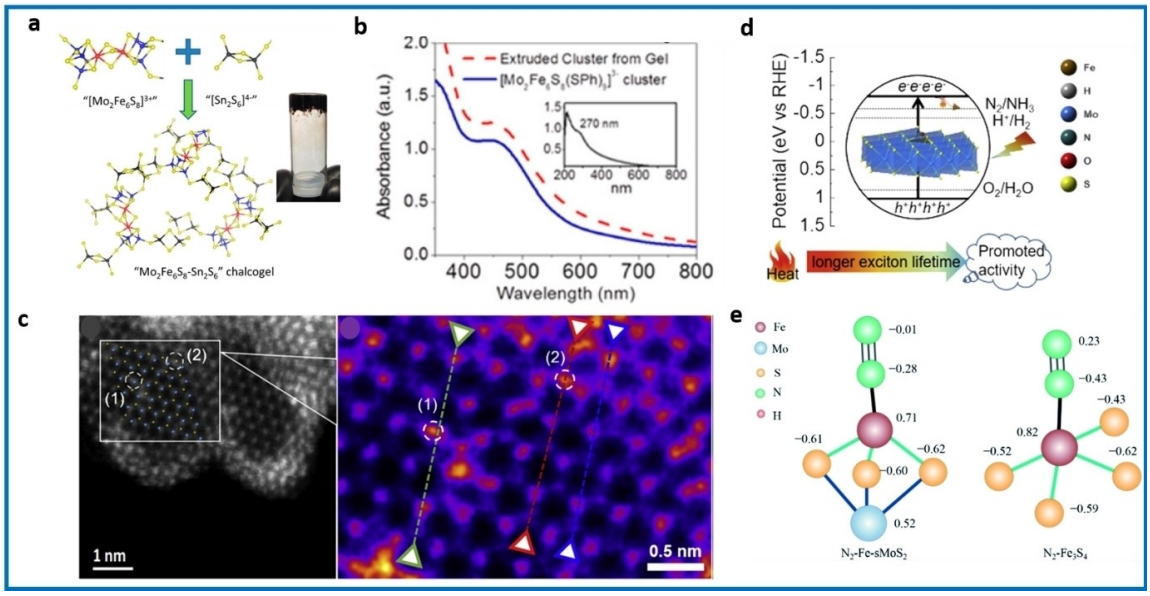

Figure 11. **(a)** Schematic representation of $Mo_2Fe_6S_8$–Sn_2S_6 biomimetic chalcogel (FeMoS-chalcogel), building block scheme (Mo, blue; Fe, red; S, yellow; Sn, black), and the picture of chalcogel shown in the right. **(b)** UV–vis spectra of $[Mo_2Fe_6S_8(SPh)_9]^{3-}$ in DMF. The inset shows the UV–vis spectra of a colloidal suspension of FeMoS–Sn_2S_6 chalcogel in water. (a-b) Reproduced with permission from Reference [135]. Copyright 2015 American Chemical Society. **(c)** HAADF-STEM image of the 2D single-layered MoS_2 ($sMoS_2$) with [Fe—S_2—Mo] [Fe–$sMoS_2$ (3 wt%)]. Atomic-resolution HAADF-STEM image of the basal plane of Fe–$sMoS_2$. Scan 1 (green line) indicates the Fe atom on a Mo atop site, scan 2 (red line) signifies the S vacancy substituted by a Fe atom, and the additional blue line also shows a Fe atom on a Mo atop site. **(d)** Correlation of activity with heat and light at pH 7 for ammonia synthesis where photoexcitation and heat can indirectly affect the activity through subsequent rate enhancements and prolonged exciton lifetime. **(c–d)** Reproduced with permission from Reference [136]. Copyright 2021 Cell Press. **(e)** Electronic structure of N_2 activation over nitrogenase-mimic Fe–$sMoS_2$ and Fe_3S_4. The presented data is the Bader charge of the corresponding atoms in units of electrons. Reproduced with permission from Reference [137]. Copyright 2020 Royal Society of Chemistry.

similar local electronic structure with enzyme nitrogenase (Figure 11e).

Overall, biomimetic catalysts show promising results in small-scale experiments and could potentially lead to more efficient and sustainable N_2 activation processes in the future. It can lead to more sustainable and efficient processes for producing fertilizers and other industrial chemicals. Table 1 shows the summarized results of materials used for photocatalytic formation of ammonia at ambient conditions.

6. Urea Synthesis

Urea is one of the important compounds for the human food chain. By 2026, the world will need 200 million metric tons of urea where 80% will be utilized as fertilizers.[138,139] Traditionally urea has been synthesized by the Bosch-Miser method. The synthesis has two steps. Step one is the reaction of liquid ammonia with gaseous carbon dioxide to form ammonium carbamate. Step two is the decomposition of ammonium carbamate into urea and water. The major issue of the prescribed reaction is that it needs harsh reaction conditions and produces a rather large carbon footprint. Over the last five years, there have therefore been numerous attempts to produce urea at ambient conditions. In this regard CO_2 and various nitrogenous compounds (such as NO_3^-, NO_2^-, N_2, and NO) have been investigated as precursors for urea synthesis via both photocatalysis and electrolysis pathways.[140–142]

In contrast to photocatalysis, the electrocatalytic path has been well advanced. For example, one of the first electrocatalytic syntheses of urea was reported in 1995 when Shibata et al. synthesized urea via the electrochemical reduction of CO_2 and NO_3^-/NO_2^- using Cu-loaded gas-diffusion electrodes.[143] Recently various metal-containing catalysts like Pd, In, Zn, and Cu have been used for urea synthesis with various nitrogen sources.[138,141] In many methods, the reactions not only enable a direct ambient synthesis of urea but the authors also manage to remove these reduced nitrogen species like urea, ammonia, and other ammonium salts from water through a reduction mechanism. Figure 12 gives an idea regarding urea synthesis on the nanomaterial surface and also explains the possibility of electrocatalytic coupling between nitrogen species and carbon dioxide to produce urea.[144] The aforementioned reaction proceeds through the catalytic active facet (100) of $In(OH)_3$ nanoparticle and C–N coupling happens through the reaction between $*NO_2$ and $*CO_2$ intermediates. This is a key step for urea synthesis because it goes through low-energy states like $*CO_2NO_2$, $*CO_2NH_2$, and $*COOHNH_2$.

In 2018, Wang et al. reported the photocatalytic synthesis of urea in 2D-CdS@3D-BiOBr heterostructures (Figure 13a).[145] BiOBr is a well-known semiconductor for photocatalytic ammonia synthesis. But in heterojunction forms of 2D-CdS@3D-BiOBr composites both the components could be excited to create electrons and holes by illumination with visible light. The effective transfer of photogenerated electrons happens from the conduction band (CB) of 3D-BiOBr into the valence band

Table 1. Summary of the reported photocatalysts for nitrogen activation with apparent quantum efficiency and quantitative yield of reduced products.

Photocatalyst	Method of Synthesis	Product	Yield	AQE	Method of Product Detection	References
F–Vo–TiO_2	Solvothermal	NH_3	206 $\mu mol\,h^{-1}g_{cat.}^{-1}$	0.38% at 420nm	NMR	[60]
Single-atom Fe-modified macro-/mesoporous TiO_2–SiO_2 (Fe–T–S)	Hydrothermal	NH_3	32 $\mu mol\,g^{-1}h^{-1}$	Not Mentioned	Nessler's Reagent	[61]
Ultrathin TiO_2 nanosheets	Hydrothermal	NH_3	1.54 $\mu mol\,g^{-1}h^{-1}$	0.08% at 600 nm	Indophenol blue and HRMS	[66]
Bi_5O_7Br nanotube	Hydrothermal	NH_3	1.38 $mmol\,h^{-1}g^{-1}$	2.3% at 420 nm	Nessler's Reagent	[77]
BiOCl NSs–Fe–5%	Hydrothermal	NH_3	1.022 $mmol\,g^{-1}h^{-1}$	1.8% at 420 nm	Indophenol blue	[78]
Bismuth monoxide (BiO) QDs	Hydrothermal	NH_3	1226 $\mu mol\,g^{-1}h^{-1}$	Not Mentioned	IR Spectroscopy	[80]
$Bi_2S_3/KTa_{0.75}Nb_{0.25}O_3$ (KTN)	Hydrothermal	NH_3	561.6 $\mu mol\,L^{-1}g^{-1}h^{-1}$	0.008%	NMR	[92]
Nanocomposite of 0D/2D $AgInS_2/Ti_3C_2$	Hydrothermal	NH_3	38.8$\mu molg^{-1}h^{-1}$	0.07% at 420nm	Indophenol blue	[93]
Ultrathin MoS_2	Hydrothermal	NH_3	325 $\mu molg^{-1}h^{-1}$	Not Mentioned	Indophenol blue	[94]
MoO_{3-x} nanosheets	Solvothermal	NH_3	328 $\mu molg^{-1}h^{-1}$	0.31% and 0.22% at 808 and 905 nm	Nessler's Reagent	[109]
MoO_{3-x} nanospheres	Aerosol-spray	NH_3	435.57 $\mu mol\,h^{-1}g^{-1}$	1.24% at 808 nm and 1.12% at 1064 nm	Nessler's Reagent	[111]
AuRu core-antenna nanostructure	Solvothermal	NH_3	101.4 $\mu mol\,g^{-1}\,h^{-1}$	0.21% and 0.17% at 350 nm and 550 nm	Ion Chromatography	[115]
Porous CuFe nanostructures	Selective Etching from solid powder	NH_3	342 $\mu mol\,g_{cat.}^{-1}\cdot h^{-1}$	0.13% at 535 nm	NMR	[116]
r-Ti_3C_2/Au	Solvothermal	NH_3	22.6 $\mu mol\,h^{-1}g_{cat}^{-1}$	0.697% at 520 nm	Nessler's Reagent	[123]
10 wt% BiOBr/Ti_3C_2	Hydrothermal	NH_3	234.6 $\mu mol\,g^{-1}h^{-1}$	2.37% at 420 nm	Nessler's Reagent	[124]
V-g-C_3N_4	Solid state then calcination	NH_3	1.24 $mmol\,g^{-1}h^{-1}$	Not Mentioned	Nessler's Reagent	[130]
B-doped g-C_3N_4 nanosheets (BCN)	Thermal	NH_3	313.9 $\mu mol\,g^{-1}h^{-1}$	0.64% at 420 nm	Nessler's Reagent	[131]
$Mo_2Fe_6S_8$–Sn_2S_6 biomimetic chalcogel	Solvothermal	NH_3	0.17 $\mu molh^{-1}$ for 1μmol of catalyst	Not Mentioned	Indophenol blue	[135]
Fe–S_2–Mo	Solvothermal	NH_3	2.1 $mmol\,g^{-1}h^{-1}$ at 270 °C	37.1% at 432 nm (270 °C)	Ammonia Gas Sensing ISE Electrode	[136]
2D-CdS@3D-BiOBr	Hydrothermal	$NH_3$and Urea	15 $\mu mol\,g^{-1}h^{-1}$	3.93% at 475 nm	Gas Chromatogram	[145]
Ti^{3+}–TiO_2/Fe–CNTs	Hydrothermal	Urea	710 $\mu mol\,L^{-1}h^{-1}$	Not Mentioned	GC-MS	[146]
Pd/LTA-3A	Microwave	Urea	87 $\mu mol\,g^{-1}h^{-1}$	Not Mentioned	LC–MS	[148]

(VB) of 2D-CdS. In addition, the 40%2D-CdS@3D-BiOBr composite exhibits a stronger photocurrent response than both the pristine 2D-CdS and the pristine 3D-BiOBr (Figure 13b) which also shows that the composite is much more effective at separating the photogenerated charges. The 40%2D-CdS/3D-BiOBr composite also shows the highest efficiency of urea formation without any sacrificial reagents.

In 2021, Maimaiti et al. reported Ti^{3+}–TiO_2/carbon nanotubes with Fe cores (Fe–CNTs) nanocomposite for efficient synthesis of urea from CO_2 and N_2 mixtures.[146] Structurally this material was prepared in two steps. First, Fe–CNTs were synthesized by the vapor deposition method. Secondly, Ti^{3+}-doped TiO_2 (Ti^{3+}–TiO_2) in brookite crystal structure was obtained via thermal reduction where $NaBH_4$ was used as a reducing agent. Then, the TiO_2 was loaded on as-prepared Fe–CNTs to obtain Ti^{3+}–TiO_2/Fe–CNTs. The composite structures absorb visible light and the vacant Ti^{3+} site actively participates in N_2 binding. The authors also have isotope-labelled product detection through mass spectra but quantitatively the yields are low. Figure 13c is a schematic of an experimental device for photocatalytic co-reduction of N_2/CO_2 to urea.

Srinivas et al. have also observed the photocatalytic urea generation in TiO_2 and Fe-titanate supported on zeolite using isopropanol/oxalic acid as the sacrificial agent and hole

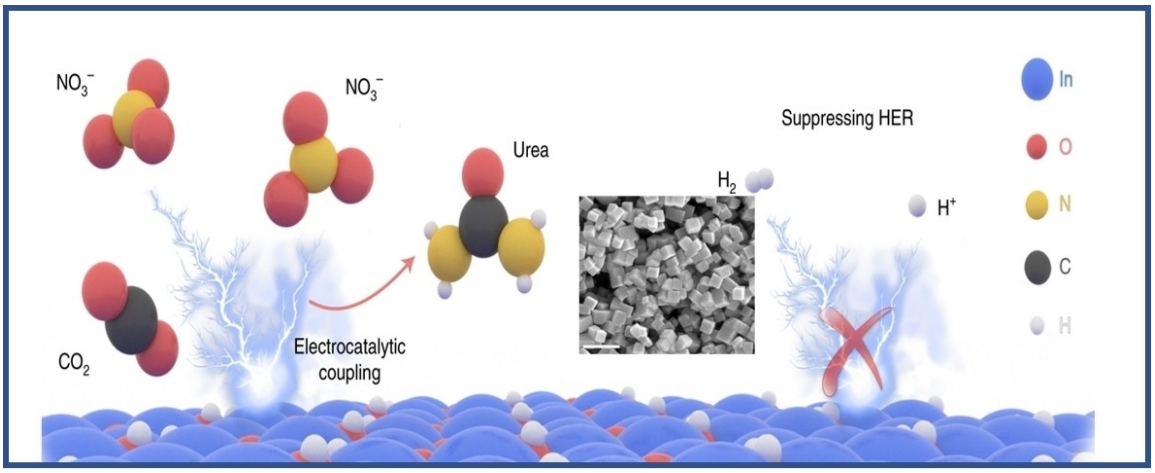

Figure 12. Schematic illustration of urea synthesis process on the surface of $In(OH)_3$ nanoparticles. Reproduced with permission from Reference [144]. Copyright 2021 Springer Nature.

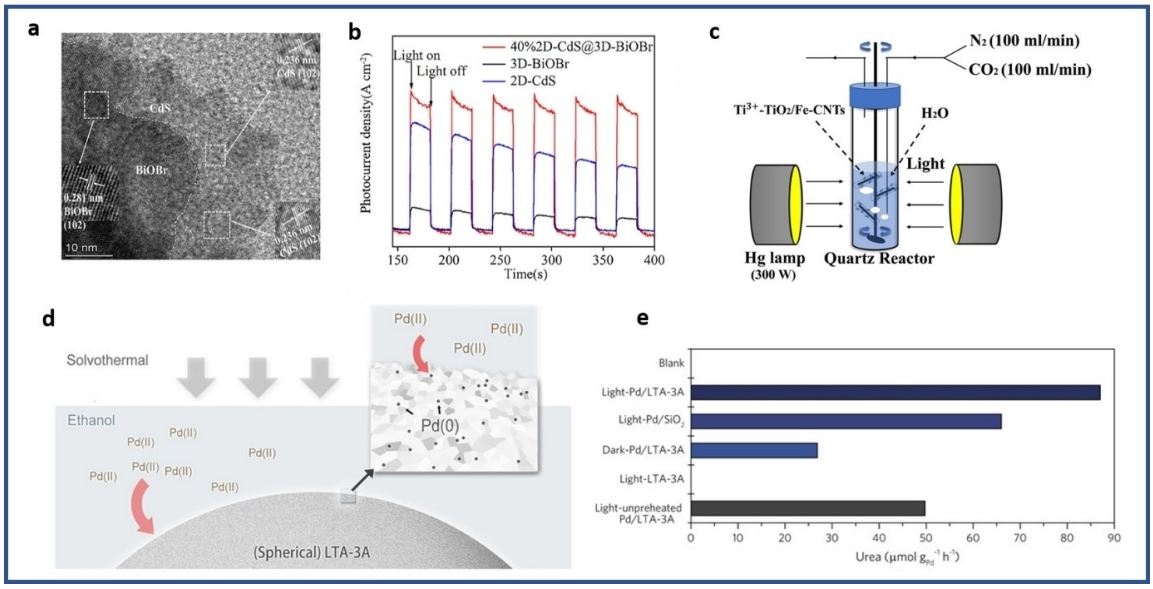

Figure 13. **(a)** HRTEM image of 40%2D-CdS@3D-BiOBr nanocomposites. **(b)** Light/dark photocurrent response of same photocatalyst samples. (a-b) Reproduced with permission from Reference [145]. Copyright 2023 American Chemical Society. **(c)** Schematic of the experimental device for photocatalytic co-reduction of N_2/CO_2 to urea. Reproduced with permission from Reference [146]. Copyright 2021 American Chemical Society. **(d)** Schematic illustration of Pd/molecular sieveLTA-3A synthesis for solar urea formation. **(e)** Catalytic performance for urea production rates under different conditions. (d–e) Reproduced with permission from Reference [148]. Copyright 2021 Wiley and Sons.

scavenger. However, the concentration of the product is very low and the mechanism is not very clear.[147]

Very recently Xia et al. have reported the solar production of urea using a Pd nanoparticle decorated molecular sieve LTA-3A.[148] Figure 13d illustrates the basic synthesis of Pd/LTA-3A. The Pd nanoparticles catalyze the reaction through dissociative adsorption where the NH_3 molecule adsorbs as Pd–NH_2 and Pd–H on the surface of two neighboring Pd atoms. Finally, CO_2 reacts with the bound –NH_2 to give urea. Different reactions with different materials (Pd on top of SiO_2 and molecular sieve) and reaction conditions (light on and off) were carried through for control reactions and Pd/LTA-3A in the presence of light shows the best catalytic performance (Figure 13e). The solar conversion rate of urea synthesis was 87 $\mu molg^{-1}h^{-1}$ and verified by isotope labeling experiments.

In conclusion, the above approaches towards photocatalytic urea synthesis are quite interesting and various catalytic materials have indeed been utilized for ambient condition urea synthesis. Nevertheless, we are still quite far from commercial applications of these methods. The main reason is that the quantitative yield is quite low and there is a clear lack of understanding of the mechanism, which in turn prevents a rational optimization of the process.

7. Amino Acids Synthesis

Very recently photo redox reactions have been considered as a powerful tool for organic C–C and C–N bond formation, but so far, only a very limited number of nanoscale catalysts have been explored for these reactions.[149–151] In this regard one of the important class of molecules for living organisms is the group of the amino acids where C–C and C–N formation happen consecutively. In this section of the review, we will discuss the recent progress of making amino acids by semiconductor nanomaterials.

In 2016, Jamison et al. reported the photo redox activation of carbon dioxide for the synthesis of amino acids in a continuous flow process. Besides the control reactions, they have also reported the formation of various amino acids with very good yields using p-terphenyl as a photo-redox catalyst.[152] Very recently König et al. have made similar examples of unnatural amino acid derivatives by activating inert C–H bonds with $Na_4W_{10}O_{32}$ (Figure 14a). To understand the reaction mechanism the author shows a radical addition pathway where after irradiation of $[W_{10}O_{32}]^{4-}$ generates a high-energy long-lived triplet excited state after intersystem crossing from the initial singlet (Figure 14b).[153]

In 2020, Song et al. reported a visible-light-driven amination of biomass-derived α-hydroxyl acids and glucose into amino acids using NH_3. The material used for this reaction was ultrathin CdS which is quite durable and stable for several reactions. The reported reaction yield was 10.5 mmol g^{-1} h^{-1} for the amino acid alanine. The authors have explained the formation of oxygen-centered radical intermediates on the ultrathin CdS nanosheets. It also lowers the activation energy barrier for the formation of amino acids, leading to high activity and good yields (Figure 14c).[154]

8. Future Prospects

8.1. Current Limitations of Photocatalytic Nitrogen Activation

8.1.1. NH_3 Detections

From all the aforementioned discussions, it is very clear that there are substantial improvements in terms of materials development both theoretically and experimentally. But currently, the photocatalytic efficiency of NRRs is not yet up to the mark for the next steps. There is a clear lack of detection and quantification the photocatalytic products like ammonia/ammonium cations. In most cases, the product has been detected through chemical reagents like Nessler reagents or Indophenol blue where there is a chance for contamination with low chemical yields.[155] In this regard NMR spectroscopy using isotope labels is quite viable. Even a proper calibration curve could quantify the results quite accurately.

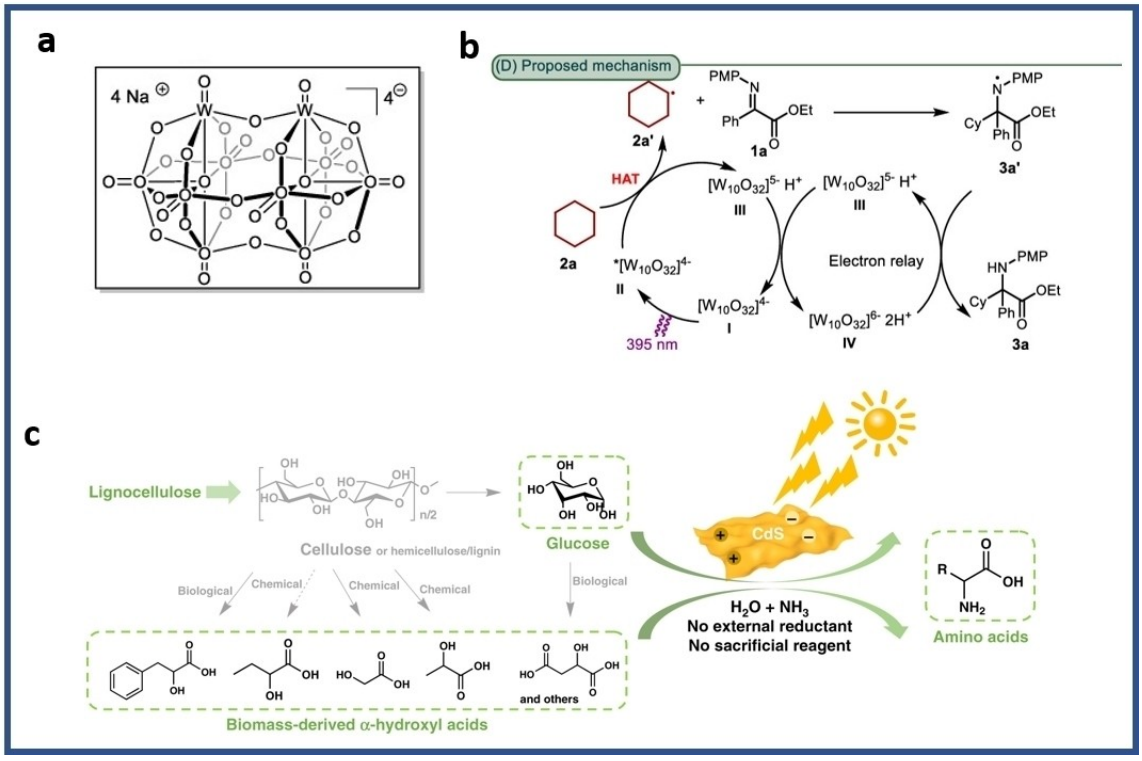

Figure 14. **(a)** Structure of the decatungstate anion used for photocatalytic synthesis of amino acids. **(b)** Proposed reaction mechanism towards amino acids. **(a–b)** Reproduced with permission from Reference [153]. Copyright 2022 American Chemical Society. **(c)** Photocatalytic amination of glucose or biomass-derived α-hydroxyl acids to amino acids. Reproduced with permission from Reference [154]. Copyright 2020 Springer Nature.

8.1.2. Proof of Intermediates and Determination of Reaction Mechanism

N_2 activation proceeds through several binding steps with various intermediates. These intermediates are often not very stable but can be detected by modern spectroscopic techniques like in situ IR spectroscopy. The spectroscopic data can also be correlated with theoretical calculations. Besides the molecular side, the photochemistry of the catalytic materials also remains elusive for most of the cases. On the other side as a plasmonic catalyst or semiconductor heterostructure, the nature of hot electrons,[156] exciton lifetime,[157] and electron transfer rate could be studied in more detail through ultrafast spectroscopy.[158,159]

8.1.3. Control Reactions

With the advancement of photocatalytic material for renewable energy applications, several precautions have been followed for control reactions. It has become a common practice for H_2 evolutions and CO_2 reduction reactions. Still, this information is quite lacking for NRR. These steps should be emphasized consecutively.(1) The first and foremost thing is whether it is a photochemical reaction or not. (2) How does the reaction go without light? (3) What is the role of a sacrificial reagent? (4) What is the stability of the catalyst during photochemical reactions?

8.2. Alternate Source of N_2

N_2 is the most abundant gas in Earth's atmosphere which can be directly utilized for photoreduction. In addition to elemental gaseous nitrogen molecules, there are other forms of nitrogen also present in the atmosphere which include various nitrogen oxides (NO_x). In general, these compounds are formed by the reaction of nitrogen and oxygen in the open atmosphere. For example, nitrogen oxides include nitrogen monoxide (NO) and nitrogen dioxide (NO_2) which play an important role in photochemical smog and acid rain formation. Another one is nitrous oxide (N_2O), a minor component of the atmosphere present at approximately 0.3 ppb. It is also a potent greenhouse gas and contributes to global warming.

Other sources of nitrogen could be deposited nitrate and nitrite salts. The deposition of nitrate salts is a naturally occurring process, generally found in little rainfall places which stops leaching out from the soil. Alternatively, nitrate is a common nitrogen species found in the atmosphere which is formed by the reaction of nitrogen dioxide (NO_2) with atmospheric oxygen (O_2). Nitrite is an intermediate nitrogen species formed during the process of nitrate reduction. It can also be formed by the reaction of nitrogen dioxide with water vapor in the atmosphere.

Nitrate reduction is a difficult process due to several reasons. The reduction of nitrate (NO_3^-) to nitrite (NO_2^-) and then to ammonia (NH_3) requires a significant amount of energy input to overcome the high activation energy barrier associated with the process. Nitrite (NO_2^-) is generally easier to reduce than N_2 because it has a lower bond strength and a lower activation energy for reduction. The bond energy of the nitrogen-nitrogen bond in nitrite is weaker than the triple bond in N_2, making it easier to break and reduce. Nitrite can be reduced to ammonia (NH_3) through photoreduction.

8.3. Advanced Materials Design

8.3.1. High Entropy Alloys

Recently, high entropy alloys (HEA) have sprung up as advanced nanomaterials for various catalytic reactions. For example, HEA nanoparticles (less than 15 nm) are showing promising activity for H_2 evolution and CO_2 reduction reactions.[160,161] Unique formation of intermetallic transition metal atoms, exceptional structure factors, enhanced surface areas, and very specific surface binding with the target molecule have made them an ideal material for these catalytic reactions.[162–164] Still, the use of HEAs in N_2 activation is quite limited. In 2021, Zhang et al. reported one of the first HEAs for electrocatalytic N_2 activation.[165] For example, uniform RuFeCoNiCu nanoparticles have been used for this purpose. Very recently there have been several theoretical findings of HEAs for N_2 activation: nitrogen adsorption and desorption are two important steps for NRR catalysts and Ti, Zr, Mo, Ru, Fe, and Au have been found to have moderate and Pd, Pt, and Ir have very good nitrogen binding activities. However, due to the hydrogen evolution activity (HER) of the noble metal atoms, they become less effective for NRR. Similarly, the surface plasmon of the metal nanoparticles becomes very important for visible light absorption. To design an advanced HEA for photocatalytic NRR the combination of nitrogen binding and surface plasmon resonance property can be an important factor. Another option could be highly mismatched alloys with a higher percentage doping of transition metals in the host semiconductor where the dopant site can act as binding of N_2 and the host semiconductor will be a light absorber.[166]

8.3.2. Single-Atom Catalysis

Single-atom catalysis has become a new avenue in heterogeneous catalytic reaction. Single atom catalysis for photocatalytic nitrogen (N_2) activation represents a cutting-edge approach in the quest for efficient and sustainable ammonia production. This technique involves the use of isolated metal atoms dispersed on a support material, which offers unique catalytic properties distinct from those of bulk or nanoparticulate catalysts. The single atom sites provide high atomic utilization efficiency and specific active sites that can facilitate the adsorption, activation, and reduction of N_2 under light irradiation. The strong metal-support interactions and the precise electronic environment around the single atoms contribute to enhanced catalytic performance, promoting efficient charge

transfer and minimizing energy losses. Up to now the single-atom catalysis of Pt, Au, and Ir have been established for various electrocatalytic reactions. In these reactions, the binding of single atoms with the substrate plays an important role.[167,168] In contrast to theoretical results,[169,170] single atom NRRs are not well known experimentally due to various factors: (1) competition between HER and NRR in certain single atom catalysts like Pd and Pt (2) controlling the distance between two single atoms side, (3) substrate binding effect in overall reactions and precise design of the active site.

Single atoms that show strong N_2 binding on a photoactive substrate may be an ideal material for NRR in the near future.[171]

8.3.3. Metal Halides

Besides the exceptional photovoltaic performance, metal halide-based perovskites are also emerging as a powerful photocatalytic material for HER and CO_2 reduction.[172,173] It acts as a perfect solar absorber in these photocatalytic reactions, even though the role of the surface binding and detailed catalytic mechanism are still not understood.[174] To our best knowledge there are no reports of photocatalytic NRR with metal halide perovskites because the surface binding of nitrogen with these materials has not been established yet. In this regard, organic-inorganic metal halides with low valent metal atoms could play an important role in nitrogen binding. Various bismuth-based perovskites and perovskites heterostructures may play a significant role in N_2 activation.[174,175]

Metal halide complexes in ionic liquids and ionic liquid template nanoparticles have been extensively studied for various catalytic applications.[176–178] The ionic liquid medium provides a unique environment for the metal complex, as it can enhance the stability and solubility of the complex while also allowing for control over the reaction conditions.[179–181] The ionic liquid can also act as a co-catalyst, providing additional functionality for the N_2 activation reaction.

Very recently two-dimensional (2D) metal halides have gained significant attention for their potential applications in catalysis.[182] These materials consist of layered metal cations (mainly transition metals, Bi and In-based) sandwiched between layers of halide anions (such as Cl, Br, or I), which form a 2D structure.[183,184] One of the key advantages of 2D metal halides for NRR is their large surface area with open metal centers for direct binding. The 2D architecture also allows for a greater number of active sites for catalytic reactions. The 2D structure provides the opportunity for tuning the electronic and optical properties of the material by changing the metal and halide components, which can be used to optimize its catalytic performance for specific photocatalytic NRR.

9. Conclusions

In this article, we have reviewed the recent progress of photocatalytic synthesis of ammonia, urea, and amino acids which are some of the key compounds for both biology and as a feedstock. Besides the various designs of novel catalytic materials, their optical properties, surface binding, and product formations have been summarized. Finally, prospects with alternative nitrogen sources, quantitative product estimation, and new emerging catalytic materials have been discussed. Photocatalytic N_2 activation is a novel approach to make N_2 useful as a fertilizer or an important chemical feedstock for future sustainable energy applications.

Acknowledgements

The authors thank the University of Potsdam (grant 53170000, A. T.), Fraunhofer Leistungszentrum Funktionsintegration, and CRC/SFB 1636 – Project ID 510943930 – Project No. Z01 (A. T., B. B.) for financial support. Prof. Lu thanks the Deutsche Forschungsgemeinschaft (DFG, German Research Foundation) CRC/SFB 1636 for financial support – Project ID 510943930 - Projects No. A02, Z01. Open Access funding enabled and organized by Projekt DEAL.

Conflict of Interests

The authors declare no conflict of interest.

Keywords: Photocatalysis · N_2 Activation · Green Energy · Sustainable Material · Ammonia

[1] J. A. Harvey, K. Tougeron, R. Gols, R. Heinen, M. Abarca, P. K. Abram, Y. Basset, M. Berg, C. Boggs, J. Brodeur, et al., *Ecol. Monogr.* **2023**, *93*(1), e1553. DOI: https://doi.org/10.1002/ecm.1553.
[2] T. R. Karl, K. E. Trenberth, *Science* **2003**, *302*(5651), 1719–1723. DOI: 10.1126/science.1090228.
[3] H. O. Pörtner, A. P. Farrell, *Science* **2008**, *322*(5902), 690–692. DOI: 10.1126/science.1163156.
[4] S. R. Loarie, P. B. Duffy, H. Hamilton, G. P. Asner, C. B. Field, D. D. Ackerly, *Nature* **2009**, *462*(7276), 1052–1055. DOI: 10.1038/nature08649.
[5] S. Anto, S. S. Mukherjee, R. Muthappa, T. Mathimani, G. Deviram, S. S. Kumar, T. N. Verma, A. Pugazhendhi, *Chemosphere* **2020**, *242*, 125079. DOI: https://doi.org/10.1016/j.chemosphere.2019.125079.
[6] A. Midilli, I. Dincer, M. Ay, *Energy Policy* **2006**, *34*(18), 3623–3633. DOI: https://doi.org/10.1016/j.enpol.2005.08.003.
[7] A. M. Omer, *Renewable Sustainable Energy Rev.* **2008**, *12*(7), 1789–1821. DOI: https://doi.org/10.1016/j.rser.2006.05.009.
[8] F. Ebeling, S. Lotz, *Nature Clim. Change* **2015**, *5*(9), 868–871. DOI: 10.1038/nclimate2681.
[9] H. B. Gray, *Nat. Chem.* **2009**, *1*(1), 7–7. DOI: 10.1038/nchem.141.
[10] D. G. Nocera, *Acc. Chem. Res.* **2017**, *50*(3), 616–619. DOI: 10.1021/acs.accounts.6b00615.
[11] J. A. Herron, J. Kim, A. A. Upadhye, G. W. Huber, C. T. Maravelias, *Energy Environ. Sci.* **2015**, *8*(1), 126–157. DOI: https://doi.org/10.1039/C4EE01958J.
[12] G. Segev, J. Kibsgaard, C. Hahn, Z. J. Xu, W.-H. Cheng, T. G. Deutsch, C. Xiang, J. Z. Zhang, L. Hammarström, D. G. Nocera, et al., *J. Phys. D* **2022**, *55*(32), 323003. DOI: 10.1088/1361-6463/ac6f97.
[13] A. Yapicioglu, I. Dincer, *Renewable Sustainable Energy Rev.* **2019**, *103*, 96–108. DOI: https://doi.org/10.1016/j.rser.2018.12.023.
[14] J. H. Montoya, L. C. Seitz, P. Chakthranont, A. Vojvodic, T. F. Jaramillo, J. K. Nørskov, *Nat. Mater.* **2017**, *16*(1), 70–81. DOI: 10.1038/nmat4778.

[15] L. Wang, M. Xia, H. Wang, K. Huang, C. Qian, C. T. Maravelias, G. A. Ozin, *Joule* **2018**, *2*(6), 1055–1074. DOI: https://doi.org/10.1016/j.joule.2018.04.017.
[16] F. Chang, W. Gao, J. Guo, P. Chen, *Adv. Mater.* **2021**, *33*(50), 2005721. DOI: https://doi.org/10.1002/adma.202005721.
[17] S. Giddey, S. P. S. Badwal, C. Munnings, M. Dolan, *ACS Sustainable Chem. Eng.* **2017**, *5*(11), 10231–10239. DOI: 10.1021/acssuschemeng.7b02219.
[18] J. W. Erisman, M. A. Sutton, J. Galloway, Z. Klimont, W. Winiwarter, *Nature Geosci.* **2008**, *1*(10), 636–639. DOI: 10.1038/ngeo325.
[19] J. Guo, P. Chen, *Nature Catalysis* **2021**, *4*(9), 734–735. DOI: 10.1038/s41929-021-00676-0.
[20] M. Capdevila-Cortada, *Nature Catalysis* **2019**, *2*(12), 1055–1055. DOI: 10.1038/s41929-019-0414-4.
[21] B. Ruscic, J. Berkowitz, *J. Chem. Phys.* **1991**, *95*(6), 4378–4384. DOI: 10.1063/1.461761.
[22] G. Glockler, *J. Chem. Phys.* **2004**, *19*(1), 124–125. DOI: 10.1063/1.1747958.
[23] J. Kim, D. C. Rees, *Biochemistry* **1994**, *33*(2), 389–397. DOI: 10.1021/bi00168a001.
[24] B. M. Hoffman, D. Lukoyanov, Z.-Y. Yang, D. R. Dean, L. C. Seefeldt, *Chem. Rev.* **2014**, *114*(8), 4041–4062. DOI: 10.1021/cr400641x.
[25] K. Tanifuji, Y. Ohki, *Chem. Rev.* **2020**, *120*(12), 5194–5251. DOI: 10.1021/acs.chemrev.9b00544.
[26] M. M. Georgiadis, H. Komiya, P. Chakrabarti, D. Woo, J. J. Kornuc, D. C. Rees, *Science* **1992**, *257*(5077), 1653–1659. DOI: 10.1126/science.1529353 (acccessed 2023/07/13).
[27] T. Spatzal, M. Aksoyoglu, L. Zhang, S. L. A. Andrade, E. Schleicher, S. Weber, D. C. Rees, O. Einsle, *Science* **2011**, *334*(6058), 940–940. DOI: 10.1126/science.1214025 (acccessed 2023/07/13).
[28] K. M. Lancaster, M. Roemelt, P. Ettenhuber, Y. Hu, M. W. Ribbe, F. Neese, U. Bergmann, S. DeBeer, *Science* **2011**, *334*(6058), 974–977. DOI: 10.1126/science.1206445 (acccessed 2023/07/13).
[29] S. F. McWilliams, P. L. Holland, *Acc. Chem. Res.* **2015**, *48*(7), 2059–2065. DOI: 10.1021/acs.accounts.5b00213.
[30] R. N. F. A. M. Dhar, *Proc. Natl. Acad. Sci. India* **1951**, *20(A)*, 112–117.
[31] G. N. Schrauzer, T. D. Guth, *J. Am. Chem. Soc.* **1977**, *99*(22), 7189–7193. DOI: 10.1021/ja00464a015.
[32] G. N. Schrauzer, N. Strampach, L. N. Hui, M. R. Palmer, J. Salehi, *Proc. Natl. Acad. Sci. USA* **1983**, *80*(12), 3873–3876. DOI: doi:10.1073/pnas.80.12.3873.
[33] T. Rayment, R. Schlögl, J. M. Thomas, G. Ertl, *Nature* **1985**, *315*(6017), 311–313. DOI: 10.1038/315311a0.
[34] N. N. Rao, S. Dube, Manjubala, P. Natarajan, *Appl. Catal. B* **1994**, *5*(1), 33–42. DOI: https://doi.org/10.1016/0926-3373(94)00042-5.
[35] M. Vettraino, M. Trudeau, A. Y. H. Lo, R. W. Schurko, D. Antonelli, *J. Am. Chem. Soc.* **2002**, *124*(32), 9567–9573. DOI: 10.1021/ja020313p.
[36] R. Shi, Y. Zhao, G. I. N. Waterhouse, S. Zhang, T. Zhang, *ACS Catal.* **2019**, *9*(11), 9739–9750. DOI: 10.1021/acscatal.9b03246.
[37] Y. Zhao, L. Zheng, R. Shi, S. Zhang, X. Bian, F. Wu, X. Cao, G. I. N. Waterhouse, T. Zhang, *Adv. Energy Mater.* **2020**, *10*(34), 2002199. DOI: https://doi.org/10.1002/aenm.202002199 (acccessed 2023/07/14).
[38] C. Ling, X. Niu, Q. Li, A. Du, J. Wang, *J. Am. Chem. Soc.* **2018**, *140*(43), 14161–14168. DOI: 10.1021/jacs.8b07472.
[39] X. Zong, H. Yan, G. Wu, G. Ma, F. Wen, L. Wang, C. Li, *J. Am. Chem. Soc.* **2008**, *130*(23), 7176–7177. DOI: 10.1021/ja8007825.
[40] K. Chang, Z. Mei, T. Wang, Q. Kang, S. Ouyang, J. Ye, *ACS Nano* **2014**, *8*(7), 7078–7087. DOI: 10.1021/nn5019945.
[41] D. J. Martin, K. Qiu, S. A. Shevlin, A. D. Handoko, X. Chen, Z. Guo, J. Tang, *Angew. Chem. Int. Ed.* **2014**, *53*(35), 9240–9245. DOI: https://doi.org/10.1002/anie.201403375.
[42] G. Wang, Z. Chen, T. Wang, D. Wang, J. Mao, *Angew. Chem. Int. Ed.* **2022**, *61*(40), e202210789. DOI: https://doi.org/10.1002/anie.202210789.
[43] Y.-X. Pan, Y. You, S. Xin, Y. Li, G. Fu, Z. Cui, Y.-L. Men, F.-F. Cao, S.-H. Yu, J. B. Goodenough, *J. Am. Chem. Soc.* **2017**, *139*(11), 4123–4129. DOI: 10.1021/jacs.7b00266.
[44] B. Bhattacharyya, A. K. Simlandy, A. Chakraborty, G. P. Rajasekar, N. B. Aetukuri, S. Mukherjee, A. Pandey, *ACS Energy Lett.* **2018**, *3*(7), 1508–1514. DOI: 10.1021/acsenergylett.8b00886.
[45] A. Mukherjee, P. Dutta, B. Bhattacharyya, G. P. Rajasekar, A. K. Simlandy, A. Pandey, *Nano Select* **2021**, *2*(5), 958–966. DOI: https://doi.org/10.1002/nano.202000219.
[46] Z. Jiang, H. Sun, T. Wang, B. Wang, W. Wei, H. Li, S. Yuan, T. An, H. Zhao, J. Yu, et al. *Energy Environ. Sci.* **2018**, *11*(9), 2382–2389. DOI: https://doi.org/10.1039/C8EE01781F.
[47] Z.-K. Xin, M.-Y. Huang, Y. Wang, Y.-J. Gao, Q. Guo, X.-B. Li, C.-H. Tung, L.-Z. Wu, *Angew. Chem. Int. Ed.* **2022**, *61*(31), e202207222. DOI: https://doi.org/10.1002/anie.202207222.
[48] G. Zhang, Y. Li, C. He, X. Ren, P. Zhang, H. Mi, *Adv. Energy Mater.* **2021**, *11*(11), 2003294, DOI: https://doi.org/10.1002/aenm.202003294.
[49] G. Zhang, C. D. Sewell, P. Zhang, H. Mi, Z. Lin, *Nano Energy* **2020**, *71*, 104645. DOI: https://doi.org/10.1016/j.nanoen.2020.104645.
[50] M. A. Shipman, M. D. Symes, *Catal. Today* **2017**, *286*, 57–68. DOI: https://doi.org/10.1016/j.cattod.2016.05.008.
[51] Q. Han, H. Jiao, L. Xiong, J. Tang, *Mater Adv* **2021**, *2*(2), 564–581. DOI: https://doi.org/10.1039/D0MA00590H.
[52] J. Yang, Y. Guo, W. Lu, R. Jiang, J. Wang, *Adv. Mater.* **2018**, *30*(48), 1802227. DOI: https://doi.org/10.1002/adma.201802227.
[53] X. Niu, A. Shi, D. Sun, S. Xiao, T. Zhang, Z. Zhou, X. a. Li, J. Wang, *ACS Catal.* **2021**, *11*(22), 14058–14066. DOI: 10.1021/acscatal.1c03407.
[54] Z. Zhao, D. Wang, R. Gao, G. Wen, M. Feng, G. Song, J. Zhu, D. Luo, H. Tan, X. Ge, et al., *Angew. Chem. Int. Ed.* **2021**, *60*(21), 11910–11918. DOI: https://doi.org/10.1002/anie.202100726.
[55] J. Chen, W. Zhang, H. Li, W. Li, D. Zhao, *SusMat* **2021**, *1*(2), 174–193. DOI: https://doi.org/10.1002/sus2.13.
[56] Y. K. Kho, A. Iwase, W. Y. Teoh, L. Mädler, A. Kudo, R. Amal, *J. Phys. Chem. C* **2010**, *114*(6), 2821–2829. DOI: 10.1021/jp910810r.
[57] S. N. Habisreutinger, L. Schmidt-Mende, J. K. Stolarczyk, *Angew. Chem. Int. Ed.* **2013**, *52*(29), 7372–7408. DOI: https://doi.org/10.1002/anie.201207199.
[58] J. Low, B. Cheng, J. Yu, *Appl. Surf. Sci.* **2017**, *392*, 658–686. DOI: https://doi.org/10.1016/j.apsusc.2016.09.093.
[59] R. Silveyra, L. De La Torre Sáenz, W. A. Flores, V. C. Martínez, A. A. Elguézabal, *Catal. Today* **2005**, *107–108*, 602–605. DOI: https://doi.org/10.1016/j.cattod.2005.07.023.
[60] R. Guan, D. Wang, Y. Zhang, C. Liu, W. Xu, J. Wang, Z. Zhao, M. Feng, Q. Shang, Z. Sun, *Appl. Catal. B* **2021**, *282*, 119580. DOI: https://doi.org/10.1016/j.apcatb.2020.119580.
[61] S. Wu, Z. Chen, W. Yue, S. Mine, T. Toyao, M. Matsuoka, X. Xi, L. Wang, J. Zhang, *ACS Catal.* **2021**, *11*(7), 4362–4371. DOI: 10.1021/acscatal.1c00072.
[62] J. Li, D. Wang, R. Guan, Y. Zhang, Z. Zhao, H. Zhai, Z. Sun, *ACS Sustainable Chem. Eng.* **2020**, *8*(49), 18258–18265. DOI: 10.1021/acssuschemeng.0c06775.
[63] M.-C. Tsai, T.-T. Nguyen, N. G. Akalework, C.-J. Pan, J. Rick, Y.-F. Liao, W.-N. Su, B.-J. Hwang, *ACS Catal.* **2016**, *6*(10), 6551–6559. DOI: 10.1021/acscatal.6b00600.
[64] N. Cao, Z. Chen, K. Zang, J. Xu, J. Zhong, J. Luo, X. Xu, G. Zheng, *Nat. Commun.* **2019**, *10*(1), 2877. DOI: 10.1038/s41467-019-10888-5.
[65] T. Wu, X. Zhu, Z. Xing, S. Mou, C. Li, Y. Qiao, Q. Liu, Y. Luo, X. Shi, Y. Zhang, et al., *Angew. Chem. Int. Ed.* **2019**, *58*(51), 18449–18453. DOI: https://doi.org/10.1002/anie.201911153.
[66] Y. Zhao, Y. Zhao, R. Shi, B. Wang, G. I. N. Waterhouse, L.-Z. Wu, C.-H. Tung, T. Zhang, *Adv. Mater.* **2019**, *31*(16), 1806482. DOI: https://doi.org/10.1002/adma.201806482.
[67] H. Hirakawa, M. Hashimoto, Y. Shiraishi, T. Hirai, *J. Am. Chem. Soc.* **2017**, *139*(31), 10929–10936. DOI: 10.1021/jacs.7b06634.
[68] Q. Liu, L. Ai, J. Jiang, *J. Mater. Chem. A* **2018**, *6*(9), 4102–4110. DOI: https://doi.org/0.1039/C7TA09350K.
[69] J. Yang, Y. Guo, R. Jiang, F. Qin, H. Zhang, W. Lu, J. Wang, J. C. Yu, *J. Am. Chem. Soc.* **2018**, *140*(27), 8497–8508. DOI: 10.1021/jacs.8b03537.
[70] M. Shi, H. Yang, Z. Zhao, G. Ren, X. Meng, *Chem. Commun.* **2023**, *59*(29), 4274–4287. DOI: https://doi.org/10.1039/D3CC00580A.
[71] Y. Huang, N. Zhang, Z. Wu, X. Xie, *J. Mater. Chem. A* **2020**, *8*(10), 4978–4995. DOI: https://doi.org/10.1039/C9TA13589H.
[72] D. Cui, L. Wang, Y. Du, W. Hao, J. Chen, *ACS Sustainable Chem. Eng.* **2018**, *6*(12), 15936–15953. DOI: 10.1021/acssuschemeng.8b04977.
[73] X. Jin, L. Ye, H. Xie, G. Chen, *Coord. Chem. Rev.* **2017**, *349*, 84–101. DOI: https://doi.org/10.1016/j.ccr.2017.08.010.
[74] J. Di, J. Xia, H. Li, S. Guo, S. Dai, *Nano Energy* **2017**, *41*, 172–192. DOI: https://doi.org/10.1016/j.nanoen.2017.09.008.
[75] J. Xiong, P. Song, J. Di, H. Li, *J. Mater. Chem. A* **2020**, *8*(41), 21434–21454. DOI: https://doi.org/10.1039/D0TA06044E.
[76] J. Di, J. Xia, M. Ji, S. Yin, H. Li, H. Xu, Q. Zhang, H. Li, *J. Mater. Chem. A* **2015**, *3*(29), 15108–15118. DOI: https://doi.org/10.1039/C5TA02388B.

[77] S. Wang, X. Hai, X. Ding, K. Chang, Y. Xiang, X. Meng, Z. Yang, H. Chen, J. Ye, *Adv. Mater.* **2017**, *29*(31), 1701774. DOI: https://doi.org/10.1002/adma.201701774.
[78] N. Zhang, L. Li, Q. Shao, T. Zhu, X. Huang, X. Xiao, *ACS Appl. Energ. Mater.* **2019**, *2*(12), 8394–8398. DOI: 10.1021/acsaem.9b01961.
[79] Q. Meng, C. Lv, J. Sun, W. Hong, W. Xing, L. Qiang, G. Chen, X. Jin, *Appl. Catal. B* **2019**, *256*, 117781. DOI: https://doi.org/10.1016/j.apcatb.2019.117781.
[80] S. Sun, Q. An, W. Wang, L. Zhang, J. Liu, W. A. Goddard Iii, *J. Mater. Chem. A* **2017**, *5*(1), 201–209. DOI: https://doi.org/10.1039/C6TA09275F.
[81] Y. Zhang, Y. Wang, X. Mou, C. Song, D. Wang, *Electrochim. Acta* **2023**, *439*, 141661. DOI: https://doi.org/10.1016/j.electacta.2022.141661.
[82] B. Rösch, T. X. Gentner, J. Langer, C. Färber, J. Eyselein, L. Zhao, C. Ding, G. Frenking, S. Harder, *Science* **2021**, *371*(6534), 1125–1128. DOI: https://doi.org/10.1126/science.abf2374.
[83] Z. Wen, H. Lv, X. Wu, *ACS Appl. Mater. Interfaces* **2022**, *14*(46), 52079–52086. DOI: 10.1021/acsami.2c18260.
[84] S. Dey, T. K. Hollis, in *Inorganics*, **2021**, Vol. 9.
[85] M.-H. Vu, M. Sakar, S. A. Hassanzadeh-Tabrizi, T.-O. Do, *Adv. Mater. Interfaces* **2019**, *6*(12), 1900091. DOI: https://doi.org/10.1002/admi.201900091.
[86] M. A. Mushtaq, A. Kumar, G. Yasin, M. Tabish, M. Arif, S. Ajmal, W. Raza, S. Naseem, J. Zhao, P. Li, et al., *Small n/a* (n/a), 2310431. DOI: https://doi.org/10.1002/smll.202310431.
[87] G. Giuffredi, T. Asset, Y. Liu, P. Atanassov, F. Di Fonzo, *ACS Materials Au* **2021**, *1*(1), 6–36. DOI: 10.1021/acsmaterialsau.1c00006.
[88] M. A. Mushtaq, M. Arif, G. Yasin, M. Tabish, A. Kumar, S. Ibraheem, W. Ye, S. Ajmal, J. Zhao, P. Li, et al., *Renewable Sustainable Energy Rev.* **2023**, *176*, 113197. DOI: https://doi.org/10.1016/j.rser.2023.113197.
[89] P. Li, Y. Liu, M. A. Mushtaq, D. Yan, *Inorg. Chem. Front.* **2023**, *10*(16), 4650–4667. DOI: https://doi.org/10.1039/D3QI00683B.
[90] M. A. Mushtaq, A. Kumar, G. Yasin, M. Arif, M. Tabish, S. Ibraheem, X. Cai, W. Ye, X. Fang, A. Saad, et al., *Appl. Catal. B* **2022**, *317*, 121711. DOI: https://doi.org/10.1016/j.apcatb.2022.121711.
[91] S. Yang, W. Ye, D. Zhang, X. Fang, D. Yan, *Inorg. Chem. Front.* **2021**, *8*(7), 1762–1770. DOI: https://doi.org/10.1039/D0QI01437K.
[92] L. Chen, X. Dai, X. Li, J. Wang, H. Chen, X. Hu, H. Lin, Y. He, Y. Wu, M. Fan, *J. Mater. Chem. A* **2021**, *9*(22), 13344–13354. DOI: https://doi.org/10.1039/D1TA02270A.
[93] J. Qin, X. Hu, X. Li, Z. Yin, B. Liu, K.-h. Lam, *Nano Energy* **2019**, *61*, 27–35. DOI: https://doi.org/10.1016/j.nanoen.2019.04.028.
[94] S. Sun, X. Li, W. Wang, L. Zhang, X. Sun, *Appl. Catal. B* **2017**, *200*, 323–329. DOI: https://doi.org/10.1016/j.apcatb.2016.07.025.
[95] B. Sun, Z. Liang, Y. Qian, X. Xu, Y. Han, J. Tian, *ACS Appl. Mater. Interfaces* **2020**, *12*(6), 7257–7269. DOI: 10.1021/acsami.9b20767.
[96] E. Cortés, *Science* **2018**, *362*(6410), 28–29. DOI: 10.1126/science.aav1133.
[97] G. Baffou, R. Quidant, *Chem. Soc. Rev.* **2014**, *43*(11), 3898–3907. DOI: https://doi.org/10.1039/C3CS60364D.
[98] E. Kazuma, Y. Kim, *Angew. Chem. Int. Ed.* **2019**, *58*(15), 4800–4808. DOI: https://doi.org/10.1002/anie.201811234.
[99] E. Cortés, W. Xie, J. Cambiasso, A. S. Jermyn, R. Sundararaman, P. Narang, S. Schlücker, S. A. Maier, *Nat. Commun.* **2017**, *8*(1), 14880. DOI: 10.1038/ncomms14880.
[100] L. Zhou, D. F. Swearer, C. Zhang, H. Robatjazi, H. Zhao, L. Henderson, L. Dong, P. Christopher, E. A. Carter, P. Nordlander, et al. *Science* **2018**, *362*(6410), 69–72. DOI: 10.1126/science.aat6967.
[101] V. Jain, R. K. Kashyap, P. P. Pillai, *Adv. Opt. Mater.* **2022**, *10*(15), 2200463. DOI: https://doi.org/10.1002/adom.202200463.
[102] Y. Zhao, H. Pan, Y. Lou, X. Qiu, J. Zhu, C. Burda, *J. Am. Chem. Soc.* **2009**, *131*(12), 4253–4261. DOI: 10.1021/ja805655b.
[103] A. Cheruvathoor Poulose, G. Zoppellaro, I. Konidakis, E. Serpetzoglou, E. Stratakis, O. Tomanec, M. Beller, A. Bakandritsos, R. Zbořil, *Nat. Nanotechnol.* **2022**, *17*(5), 485–492. DOI: 10.1038/s41565-022-01087-3.
[104] B. Bhattacharyya, C. Balischewski, C. Pacholski, A. Pandey, I. Bald, A. Taubert, *Adv. Opt. Mater.* **2023**, *11*(8), 2202411. DOI: https://doi.org/10.1002/adom.202202411.
[105] R. Yadav, B. Bhattacharyya, S. K. Saha, P. Dutta, P. Roy, G. P. Rajasekar, A. Narayan, A. Pandey, *J. Phys. Chem. C* **2021**, *125*(4), 2511–2518. DOI: 10.1021/acs.jpcc.0c09009.
[106] B. Bhattacharyya, A. Pandey, *J. Am. Chem. Soc.* **2016**, *138*(32), 10207–10213. DOI: 10.1021/jacs.6b04981.
[107] A. Sugathan, B. Bhattacharyya, V. V. R. Kishore, A. Kumar, G. P. Rajasekar, D. D. Sarma, A. Pandey, *J. Phys. Chem. Lett.* **2018**, *9*(4), 696–701. DOI: 10.1021/acs.jpclett.7b03190.
[108] S. Li, P. Miao, Y. Zhang, J. Wu, B. Zhang, Y. Du, X. Han, J. Sun, P. Xu, *Adv. Mater.* **2021**, *33*(6), 2000086. DOI: https://doi.org/10.1002/adma.202000086.
[109] H. Wu, X. Li, Y. Cheng, Y. Xiao, R. Li, Q. Wu, H. Lin, J. Xu, G. Wang, C. Lin, et al., *J. Mater. Chem. A* **2020**, *8*(5), 2827–2835. DOI: https://doi.org/10.1039/C9TA13038A.
[110] J. M. P. Martirez, E. A. Carter, *ACS Nano* **2016**, *10*(2), 2940–2949. DOI: 10.1021/acsnano.6b00085.
[111] H. Bai, S. H. Lam, J. Yang, X. Cheng, S. Li, R. Jiang, L. Shao, J. Wang, *Adv. Mater.* **2022**, *34*(2), 2104226. DOI: https://doi.org/10.1002/adma.202104226.
[112] M. Thangamuthu, C. Santschi, O. J. F. Martin, *Faraday Discuss.* **2019**, *214*(0), 399–415, DOI: https://doi.org/10.1039/C8FD00146D.
[113] H. Jia, A. Du, H. Zhang, J. Yang, R. Jiang, J. Wang, C.-y. Zhang, *J. Am. Chem. Soc.* **2019**, *141*(13), 5083–5086. DOI: 10.1021/jacs.8b13062.
[114] H. Zeng, S. Terazono, T. Tanuma, *Catalysis Commun.* **2015**, *59*, 40–44. DOI: https://doi.org/10.1016/j.catcom.2014.09.034.
[115] C. Hu, X. Chen, J. Jin, Y. Han, S. Chen, H. Ju, J. Cai, Y. Qiu, C. Gao, C. Wang, et al., *J. Am. Chem. Soc.* **2019**, *141*(19), 7807–7814. DOI: 10.1021/jacs.9b01375.
[116] T. Hou, L. Chen, Y. Xin, W. Zhu, C. Zhang, W. Zhang, S. Liang, L. Wang, *ACS Energy Lett.* **2020**, *5*(7), 2444–2451. DOI: 10.1021/acsenergylett.0c00959.
[117] J. M. P. Martirez, E. A. Carter, *Sci. Adv.* **2017**, *3*(12), eaao4710. DOI: 10.1126/sciadv.aao4710.
[118] S. Saha, S. Ghoshal, P. Sarkar, *J. Chem. Sci.* **2023**, *135*(2), 48. DOI: 10.1007/s12039-023-02169-y.
[119] L. Huang, X. Gu, G. Zheng, *Chem* **2019**, *5*(1), 15–17. DOI: https://doi.org/10.1016/j.chempr.2018.12.015.
[120] L. R. Johnson, S. Sridhar, L. Zhang, K. D. Fredrickson, A. S. Raman, J. Jang, C. Leach, A. Padmanabhan, C. C. Price, N. C. Frey, et al., *ACS Catal.* **2020**, *10*(1), 253–264. DOI: 10.1021/acscatal.9b01925.
[121] K. Chu, X. Li, Q. Li, Y. Guo, H. Zhang, *Small* **2021**, *17*(40), 2102363. DOI: https://doi.org/10.1002/smll.202102363.
[122] K. Chu, X. Li, Y. Tian, Q. Li, Y. Guo, *Energy Environ. Mater.* **2022**, *5*(4), 1303–1309. DOI: https://doi.org/10.1002/eem2.12247.
[123] B. Chang, Y. Guo, D. Wu, L. Li, B. Yang, J. Wang, *Chem. Sci.* **2021**, *12*(33), 11213–11224. DOI: https://doi.org/10.1039/D1SC02772G.
[124] Y. Fang, Y. Cao, B. Tan, Q. Chen, *ACS Appl. Mater. Interfaces* **2021**, *13*(36), 42624–42634. DOI: 10.1021/acsami.1c08888.
[125] J. Fu, J. Yu, C. Jiang, B. Cheng, *Adv. Energy Mater.* **2018**, *8*(3), 1701503. DOI: https://doi.org/10.1002/aenm.201701503.
[126] P. Li, Y. Lin, Z. Qi, D. Yan, *J. Mater. Chem. A* **2023**, *11*(39), 21078–21088. DOI: https://doi.org/10.1039/D3TA03285J.
[127] S. Wang, L. Shi, X. Bai, Q. Li, C. Ling, J. Wang, *ACS Cent. Sci.* **2020**, *6*(10), 1762–1771. DOI: 10.1021/acscentsci.0c00552.
[128] S. Ghoshal, A. Ghosh, P. Roy, B. Ball, A. Pramanik, P. Sarkar, *ACS Catal.* **2022**, *12*(24), 15541–15575. DOI: 10.1021/acscatal.2c04527.
[129] M. Zheng, X. Cai, Y. Li, K. Ding, Y. Zhang, W. Chen, C. Sun, W. Lin, *2D Mater.* **2022**, *9*(4), 045035. DOI: 10.1088/2053-1583/ac953a.
[130] G. Dong, W. Ho, C. Wang, *J. Mater. Chem. A* **2015**, *3*(46), 23435–23441. DOI: https://doi.org/10.1039/C5TA06540B.
[131] W. Wang, H. Zhou, Y. Liu, S. Zhang, Y. Zhang, G. Wang, H. Zhang, H. Zhao, *Small* **2020**, *16*(13), 1906880. DOI: https://doi.org/10.1002/smll.201906880.
[132] W. Ye, Y. Yang, M. Arif, S. Yang, X. Fang, M. A. Mushtaq, X. Chen, D. Yan, *ACS Sustainable Chem. Eng.* **2020**, *8*(42), 15946–15952. DOI: 10.1021/acssuschemeng.0c05523.
[133] T. M. Buscagan, D. C. Rees, *Joule* **2019**, *3*(11), 2662–2678. DOI: https://doi.org/10.1016/j.joule.2019.09.004.
[134] W.-J. Wei, P. E. M. Siegbahn, *Chem. Eur. J.* **2022**, *28*(12), e202103745. DOI: https://doi.org/10.1002/chem.202103745.
[135] A. Banerjee, B. D. Yuhas, E. A. Margulies, Y. Zhang, Y. Shim, M. R. Wasielewski, M. G. Kanatzidis, *J. Am. Chem. Soc.* **2015**, *137*(5), 2030–2034. DOI: 10.1021/ja512491v.
[136] J. Zheng, S. Wu, L. Lu, C. Huang, P.-L. Ho, A. Kirkland, T. Sudmeier, R. Arrigo, D. Gianolio, S. C. Edman Tsang, *Chem. Sci.* **2021**, *12*(2), 688–695. DOI: https://doi.org/10.1039/D0SC04575F.
[137] J. Zheng, L. Lu, K. Lebedev, S. Wu, P. Zhao, I. J. McPherson, T.-S. Wu, R. Kato, Y. Li, P.-L. Ho, et al., *Chem Catalysis* **2021**, *1*(1), 162–182. DOI: https://doi.org/10.1016/j.checat.2021.03.002.

[138] C. Lv, C. Lee, L. Zhong, H. Liu, J. Liu, L. Yang, C. Yan, W. Yu, H. H. Hng, Z. Qi, et al., *ACS Nano* **2022**, *16*(5), 8213–8222. DOI: 10.1021/acsnano.2c01956.
[139] X. Zhu, X. Zhou, Y. Jing, Y. Li, *Nat. Commun.* **2021**, *12*(1), 4080. DOI: 10.1038/s41467-021-24400-5.
[140] C. Chen, N. He, S. Wang, *Small Sci.* **2021**, *1*(11), 2100070. DOI: https://doi.org/10.1002/smsc.202100070.
[141] M. Jiang, M. Zhu, M. Wang, Y. He, X. Luo, C. Wu, L. Zhang, Z. Jin, *ACS Nano* **2023**, *17*(4), 3209–3224. DOI: 10.1021/acsnano.2c11046.
[142] X. Zhang, X. Zhu, S. Bo, C. Chen, M. Qiu, X. Wei, N. He, C. Xie, W. Chen, J. Zheng, et al., *Nat. Commun.* **2022**, *13*(1), 5337. DOI: 10.1038/s41467-022-33066-6.
[143] M. Shibata, K. Yoshida, N. Furuya, *J. Electroanal. Chem.* **1995**, *387*(1), 143–145. DOI: https://doi.org/10.1016/0022-0728(95)03992-P.
[144] C. Lv, L. Zhong, H. Liu, Z. Fang, C. Yan, M. Chen, Y. Kong, C. Lee, D. Liu, S. Li, et al., *Nat Sustain.* **2021**, *4*(10), 868–876. DOI: 10.1038/s41893-021-00741-3.
[145] Y. Wang, S. Wang, J. Gan, J. Shen, Z. Zhang, H. Zheng, X. Wang, *ACS Sustainable Chem. Eng.* **2023**, *11*(5), 1962–1973. DOI: 10.1021/acssuschemeng.2c06827.
[146] H. Maimaiti, B. Xu, J.-y. Sun, L.-r. Feng, *ACS Sustainable Chem. Eng.* **2021**, *9*(20), 6991–7002. DOI: 10.1021/acssuschemeng.1c00644.
[147] .B. Srinivas, V. D. Kumari, G. Sadanandam, C. Hymavathi, M. Subrahmanyam, B. R. De, *Photochem. Photobiol.* **2012**, *88*(2), 233–241. DOI: https://doi.org/10.1111/j.1751-1097.2011.01037.x; (accessed 2023/07/17).
[148] M. Xia, C. Mao, A. Gu, A. A. Tountas, C. Qiu, T. E. Wood, Y. F. Li, U. Ulmer, Y. Xu, C. J. Viasus, et al., *Angew. Chem. Int. Ed.* **2022**, *61*(1), e202110158. DOI: https://doi.org/10.1002/anie.202110158.
[149] N. E. S. Tay, D. Lehnherr, T. Rovis, *Chem. Rev.* **2022**, *122*(2), 2487–2649. DOI: 10.1021/acs.chemrev.1c00384.
[150] M. H. Shaw, J. Twilton, D. W. C. MacMillan, *J. Org. Chem.* **2016**, *81*(16), 6898–6926. DOI: 10.1021/acs.joc.6b01449.
[151] A. Y. Chan, I. B. Perry, N. B. Bissonnette, B. F. Buksh, G. A. Edwards, L. I. Frye, O. L. Garry, M. N. Lavagnino, B. X. Li, Y. Liang, et al., *Chem. Rev.* **2022**, *122*(2), 1485–1542. DOI: 10.1021/acs.chemrev.1c00383.
[152] H. Seo, M. H. Katcher, T. F. Jamison, *Nat. Chem.* **2017**, *9*(5), 453–456. DOI: 10.1038/nchem.2690.
[153] F. Babawale, K. Murugesan, R. Narobe, B. König, *Org. Lett.* **2022**, *24*(26), 4793–4797. DOI: 10.1021/acs.orglett.2c01822.
[154] S. Song, J. Qu, P. Han, M. J. Hülsey, G. Zhang, Y. Wang, S. Wang, D. Chen, J. Lu, N. Yan, *Nat. Commun.* **2020**, *11*(1), 4899. DOI: 10.1038/s41467-020-18532-3.
[155] Y. Zhao, R. Shi, X. Bian, C. Zhou, Y. Zhao, S. Zhang, F. Wu, G. I. N. Waterhouse, L.-Z. Wu, C.-H. Tung, et al., *Adv. Sci.* **2019**, *6*(8), 1802109. DOI: https://doi.org/10.1002/advs.201802109.
[156] P. Roy, A. Mukherjee, P. Mondal, B. Bhattacharyya, A. Narayan, A. Pandey, *J. Phys. Chem. C* **2022**, *126*(17), 7364–7373. DOI: 10.1021/acs.jpcc.1c10922.
[157] B. Bhattacharyya, A. Mukherjee, R. Mahadevu, A. Pandey, *J. Chem. Phys.* **2021**, *154*(7). DOI: 10.1063/5.0036676.
[158] A. K. Simlandy, B. Bhattacharyya, A. Pandey, S. Mukherjee, *ACS Catal.* **2018**, *8*(6), 5206–5211. DOI: 10.1021/acscatal.8b01078.
[159] A. Mukherjee, B. Bhattacharyya, A. Pandey, *Nano Futur.* **2018**, *2*(4), 045007. DOI: 10.1088/2399-1984/aae05a.
[160] E. P. George, D. Raabe, R. O. Ritchie, *Nat. Rev. Mater.* **2019**, *4*(8), 515–534. DOI: 10.1038/s41578-019-0121-4.
[161] T. Wang, Y. Wang, N. Wang, S. Xu, Z. Han, Y. Wang, *Mater. Lett.* **2021**, *283*, 128817. DOI: https://doi.org/10.1016/j.matlet.2020.128817.
[162] Y. Xin, S. Li, Y. Qian, W. Zhu, H. Yuan, P. Jiang, R. Guo, L. Wang, *ACS Catal.* **2020**, *10*(19), 11280–11306. DOI: 10.1021/acscatal.0c03617.
[163] N. Kumar Katiyar, K. Biswas, J.-W. Yeh, S. Sharma, C. Sekhar Tiwary, *Nano Energy* **2021**, *88*, 106261. DOI: https://doi.org/10.1016/j.nanoen.2021.106261.
[164] K. Mori, N. Hashimoto, N. Kamiuchi, H. Yoshida, H. Kobayashi, H. Yamashita, *Nat. Commun.* **2021**, *12*(1), 3884. DOI: 10.1038/s41467-021-24228-z.
[165] D. Zhang, H. Zhao, X. Wu, Y. Deng, Z. Wang, Y. Han, H. Li, Y. Shi, X. Chen, S. Li, et al., *Adv. Funct. Mater.* **2021**, *31*(9), 2006939. DOI: https://doi.org/10.1002/adfm.202006939.
[166] B. Bhattacharyya, K. Gahlot, R. Viswanatha, A. Pandey, *J. Phys. Chem. Lett.* **2018**, *9*(3), 635–640. DOI: 10.1021/acs.jpclett.7b03087.
[167] A. Wang, J. Li, T. Zhang, *Nat Rev Chem* **2018**, *2*(6), 65–81. DOI: 10.1038/s41570-018-0010-1.
[168] S. Liang, C. Hao, Y. Shi, *ChemCatChem* **2015**, *7*(17), 2559–2567. DOI: https://doi.org/10.1002/cctc.201500363.
[169] Z. Ma, Z. Cui, C. Xiao, W. Dai, Y. Lv, Q. Li, R. Sa, *Nanoscale* **2020**, *12*(3), 1541–1550. DOI: https://doi.org/10.1039/C9NR08969A.
[170] S. Tang, Q. Dang, T. Liu, S. Zhang, Z. Zhou, X. Li, X. Wang, E. Sharman, Y. Luo, J. Jiang, *J. Am. Chem. Soc.* **2020**, *142*(45), 19308–19315. DOI: 10.1021/jacs.0c09527.
[171] Z. W. Chen, Z. Lu, L. X. Chen, M. Jiang, D. Chen, C. V. Singh, *Chem Catalysis* **2021**, *1*(1), 183–195. DOI: https://doi.org/10.1016/j.checat.2021.03.003.
[172] K. Ren, S. Yue, C. Li, Z. Fang, K. A. M. Gasem, J. Leszczynski, S. Qu, Z. Wang, M. Fan, *J. Mater. Chem. A* **2022**, *10*(2), 407–429, DOI: https://doi.org/10.1039/D1TA09148D.
[173] H. Huang, B. Pradhan, J. Hofkens, M. B. J. Roeffaers, J. A. Steele, *ACS Energy Lett.* **2020**, *5*(4), 1107–1123. DOI: 10.1021/acsenergylett.0c00058.
[174] S. Chen, H. Yin, P. Liu, Y. Wang, H. Zhao, *Adv. Mater.* **2023**, *35*(6), 2203836. DOI: https://doi.org/10.1002/adma.202203836.
[175] K. S. Schanze, P. V. Kamat, P. Yang, J. Bisquert, *ACS Energy Lett.* **2020**, *5*(8), 2602–2604. DOI: 10.1021/acsenergylett.0c01480.
[176] N. Kapernaum, A. Lange, M. Ebert, M. A. Grunwald, C. Haege, S. Marino, A. Zens, A. Taubert, F. Giesselmann, S. Laschat, *ChemPlusChem* **2022**, *87*(1), e202100397. DOI: https://doi.org/10.1002/cplu.202100397.
[177] C. Balischewski, H.-S. Choi, K. Behrens, A. Beqiraj, T. Körzdörfer, A. Geßner, A. Wedel, A. Taubert, *ChemistryOpen* **2021**, *10*(2), 272–295. DOI: https://doi.org/10.1002/open.202000357.
[178] A. Abouserie, G. A. El-Nagar, B. Heyne, C. Günter, U. Schilde, M. T. Mayer, S. Stojkovikj, C. Roth, A. Taubert, *ACS Appl. Mater. Interfaces* **2020**, *12*(47), 52560–52570. DOI: 10.1021/acsami.0c13927.
[179] C. Balischewski, K. Behrens, K. Zehbe, C. Günter, S. Mies, E. Sperlich, A. Kelling, A. Taubert, *Chem. Eur. J.* **2020**, *26*(72), 17504–17513, DOI: https://doi.org/10.1002/chem.202003097.
[180] C. Balischewski, B. Bhattacharyya, E. Sperlich, C. Günter, A. Beqiraj, T. Klamroth, K. Behrens, S. Mies, A. Kelling, S. Lubahn, et al., *Chem. Eur. J.* **2022**, *28*(64), e202201068, DOI: https://doi.org/10.1002/chem.202201068.
[181] C. Balischewski, B. Bhattacharyya, J. J. Bailey, S. D. Place, P. Nockemann, J. Kim, A. Wedel, S. Gahlaut, I. Bald, W. Li, et al., *Adv. Funct. Mater.* **2024**, *34*(12), 2311571. DOI: https://doi.org/10.1002/adfm.202311571.
[182] X. Huang, L. Yan, Y. Zhou, Y. Wang, H.-Z. Song, L. Zhou, *J. Phys. Chem. Lett.* **2021**, *12*(1), 525–531. DOI: 10.1021/acs.jpclett.0c03138.
[183] A. Aji Suleiman, X. Zhou, T. Zhai, *J. Phys. D* **2021**, *54*(1), 013002. DOI: 10.1088/1361-6463/abae35.
[184] B. Bhattacharyya, C. Balischewski, E. Sperlich, C. Günter, S. Mies, A. Kelling, A. Taubert, *Adv. Mater. Interfaces* **2023**, *10*(12), 2202363, DOI: https://doi.org/10.1002/admi.202202363.

Manuscript received: April 4, 2024
Revised manuscript received: June 15, 2024
Accepted manuscript online: June 17, 2024
Version of record online: August 7, 2024